Available online at www.sciencedirect.com
SCIENCE DIRECT®
ELSEVIER
European Journal of Mechanics B/Fluids 21 (2002) 615–641

Traveling gravity water waves in two and three dimensions

Walter Craig [a,*], David P. Nicholls [b]

[a] *Department of Mathematics, McMaster University, Hamilton, Ontario L8S 4K1, Canada*
[b] *Department of Mathematics, University of Notre Dame, Canada*

Received 21 January 2002; accepted 22 August 2002

Abstract

This paper discusses the bifurcation theory for the equations for traveling surface water waves, based on the formulation of Zakharov [58] and of Craig and Sulem [15] in terms of integro-differential equations on the free surface. This theory recovers the well-known picture of bifurcation curves of Stokes progressive wavetrains in two-dimensions, with the bifurcation parameter being the phase velocity of the solution. In three dimensions the phase velocity is a two-dimensional vector, and the resulting bifurcation equations describe two-dimensional bifurcation surfaces, with multiple intersections at simple bifurcation points. The integro-differential formulation on the free surface is posed in terms of the Dirichlet–Neumann operator for the fluid domain. This lends itself naturally to numerical computations through the fast Fourier transform and surface spectral methods, which has been implemented in Nicholls [32]. We present a perturbation analysis of the resulting bifurcation surfaces for the three-dimensional problem, some analytic results for these bifurcation problems, and numerical solutions of the surface water waves problem, based on a numerical continuation method which uses the spectral formulation of the problem in surface variables. Our numerical results address the problem in both two and three dimensions, and for both the shallow and deep water cases. In particular we describe the formation of steep hexagonal traveling wave patterns in the three-dimensional shallow water regime, and their transition to rolling waves, on high aspect ratio rectangular patterns as the depth increases to infinity.

1. Introduction

In this paper we give an analysis of traveling or progressive wave solutions to the problem of free surface water waves. This is the problem for the Euler equations of an ideal fluid with a free surface, evolving under the influence of gravity in a fluid domain of infinite horizontal extent and of depth h, where $0 < h \leqslant \infty$. We work with the Hamiltonian formulation of the problem due originally to Zakharov [54], which can be written as integro-diferential equations on the free surface [18], involving the Dirichlet–Neumann operator for the fluid domain. In the two-dimensional case, we consider solutions that are periodic in the horizontal variable, and in the three-dimensional case we consider solutions that are doubly-periodic in the two horizontal variables. These are bifurcation problems, with the bifurcation parameter being the horizontal phase velocity of the solution. In the two-dimensional problem the analysis gives the classical bifurcation branches of parametrized curves of solutions that have been studied since the time of Stokes [45]. In three dimensions the bifurcation parameter is two-dimensional, and our analysis describes solution branches in the form of bifurcation surfaces. Our goals are to describe the structure of the bifurcation branches, at least in a neighborhood of simple bifurcation points, and to numerically compute traveling wave solutions along these branches, using numerical continuation methods and their higher dimensional analogs [1,53]. Where possible we continue branches of solutions up to large amplitude and large steepness, and in particular in the two-dimensional case we compute up to the Stokes wavetrain of extremal form.

* Corresponding author.
E-mail address: craig@math.mcmaster.ca (W. Craig).

0997-7546/02/$ – see front matter
PII: S0997-7546(02)01207-4

The contributions of this paper include, first of all, a perturbation analysis of the bifurcation problem for traveling surface water waves. For the two-dimensional problem, this analysis is well known, and dates essentially to the work of Stokes [45]. The perturbation calculation for the three-dimensional problem is new, and is particularly interesting as it describes the structure of the basic bifurcation surfaces of solutions and their intersections in a neighborhood of a simple bifurcation point. Secondly, we present numerical computations of certain interesting classes of two and three-dimensional traveling surface water waves. For this purpose we have developed a surface spectral method based on the surface integral formulation for the Euler equations, along the lines of [18], and using descriptions of the Dirichlet–Neumann operator that are given in [18,32,33]. And thirdly, we give analytic results on the structure of the set of solutions to bifurcation problems with multiple parameters, as in the three-dimensional case, which describes the form of the intersection of bifurcation surfaces in a neighborhood of a simple bifurcation point. In resonant cases the bifurcation is no longer simple, and the structure of solutions can be different, nonetheless we expect that solution branches will continue to exist, due to the Hamiltonian form of the problem [15] and the close relation of the problem to the resonant Lyapunov center theorem. The details of the numerical method are described in Nicholls [33], and some of the basic results on shallow water hexagonal waves and rolling waves, on high aspect ratio rectangular patterns in deep water waves are outlined in Nicholls [34].

In the two-dimensional case the problem of traveling surface water waves fits into the usual framework of a bifurcation problem with one-dimensional parameter space, for which one seeks solutions in the form of bifurcation branches of one-dimensional curves. These have been extensively studied with perturbation methods, and there have been many rigorous analytic results of existence of bifurcation branches, starting with the perturbative results of Nekrasov [31], Levi-Civita [27] and Struik [46]. A rigorous study of global aspects of the bifurcation theory, including a sketch of the global picture of the bifurcation branches, and an analysis of the extreme form of traveling wave solutions including the famous Lipschitz singularity at the stagnation point at the highest crests, has been undertaken by Amick and Toland [2]. Contributions to the theory of stability of these solution branches include the work of Plotnikov [38] on the solitary wave, and the extension of this analysis to the periodic case by Buffoni, Dancer and Toland [6].

There have been many numerical studies of the two-dimensional problem as well, and we mention in particular the following: Chen and Saffman [9,10] found secondary branches of subharmonic bifurcations in deep water ($h = +\infty$) which are continued up to solutions for which some or all of the crests have Lipschitz continuous peaks, see also [26,50–52]. Zufiria described higher order subharmonic bifurcations of solutions, ultimately computing branches of non-symmetric wave profiles of three or more times the original period; these were in the context of deep water [56] and in long wave models with finite depth [55]. Detailed studies of the singular crest in the Stokes 'wave of extremal form' have often been studied in the context of the solitary wave; we cite in particular Tanaka [49], Hunter and Vanden Broeck [23] and Longuet-Higgins and Tanaka [28]. The results above show that the Lipschitz crested wave of extremal form on a bifurcation curve is neither the solution in the family with maximal phase velocity c nor the solution with the largest slope $|\eta|_{C^1}$. The phenomenon of a turning point in the amplitude-phase velocity plane, often placed quite high on the bifurcation branch, above which the phase speed *decreases* with the amplitude of the solution, is known as the 'Tanaka instability' [49]; this is precisely the subject of the rigorous analysis of Plotnikov [38] and Buffoni, Dancer and Toland [6]. An article by Dias and Kharif [19] in the Annual Review of Fluid Mechanics gives an extensive bibliography and description of the details of this work.

In our work in the two-dimensional case, the bifurcation analysis and the application of numerical continuation methods recovers the branch of the Stokes periodic wavetrain, starting from the initial bifurcation point from uniform flow, and continuing up the branch to wave profiles of extremal form with the famous Lipschitz singular crest of angle $2\pi/3$. This branch exhibits the Tanaka phenomenon. We also observe subharmonic bifurcation from this branch of solutions, which themselves extend to surface profiles of extremal form, with alternating smooth and Lipschitz singular crests. We note that along the main secondary bifurcation branch that we have studied in detail, the phase speed of the solution *decreases uniformly* along the branch with increasing amplitude. This extends the picture described in Chen and Saffman [9] to the finite depth regime, it gives portions of the bifurcation picture of the small amplitude bifurcation diagram described by Zufiria [55,56], and it is consistent with the numerical observations of Baesens and MacKay [4] on the behavior of the phase speed as a function of amplitude. Despite the fact that our methods are designed for general two- and three-dimensional problems, and are not specialized to resolve the form of a Lipschitz crest, nonetheless the numerical solutions converge quite well, even up to the solutions of extremal form.

The three-dimensional problem is less extensively studied, and the theory of traveling wave solutions is still incomplete, either from the point of view of perturbation theory, numerical simulations or rigorous analysis. It has a basic feature that is different from the two-dimensional case, in that solutions occur in the form of two-dimensional bifurcation surfaces, and the singularity of the intersection of such surfaces at simple bifurcation points is more complex. This fact seems not to have been recognized until recently [15]. Particular curves on these bifurcation surfaces can be specified by restricting solutions under special conditions of symmetry, such as symmetric diamonds or reflection symmetry orthogonal to the direction of propagation. For example, there are recent results of formal perturbation analysis given in Bridges, Dias and Menasce [5], describing certain classes of steady three-dimensional water wave patterns, which are in this category of special curves of solutions. The paper gives a cohesive analysis which describes in a uniform manner the classes of doubly-periodic short crested steady waves and

oblique traveling waves (or Stokes wavetrains). These are, however, not all of the solutions, and a priori restrictions on the phase velocity omit information such as the dimension and the connectivity of solution branches. There have been extensive numerical studies of three-dimensional surface water waves throughout the 1980's and 1990's, for examples we cite the articles of Meiron, Saffman and Yuen [30], Roberts [40], Roberts and Peregrine [41], Saffman and Yuen [42]. In cases of surface water waves in finite but relatively shallow depth, for which the periodic fundamental domain $\mathbf{T} \subseteq \mathbf{R}^2(x)$ has large aspect ratio, and is oriented approximately orthogonally to the phase velocity $c \in \mathbf{R}^2(c)$, solutions exhibit a number of nonlinear effects, one of which is that periodic wave fields tend to form hexagonal patterns. This has been studied in the long-wave KP asymptotic regime by Hammack et al. [22,21], and by several approaches to approximating Euler flow by Milewski and Keller [29] and by the present authors [33,15]. Recent results include the experimental and numerical work of Kimmoun, Branger and Kharif [25], who consider three-dimensional surface waves over symmetric diamond periodic fundamental domains (see [39]) which in most cases have aspect ratio approximately unity, and the experimental observations of Hammack and Henderson [8] in which the aspect ratio of the fundamental domain is one of the experimental parameters.

In the present paper we describe the character of the bifurcation surfaces in a neighborhood of a simple bifurcation point, and we present a number of numerical calculations of the bifurcation surfaces, mapping a neighborhood of the bifurcation point in essentially pseudo-geodesic polar coordinates. In contrast to the many rigorous results on the existence of two-dimensional gravity waves, there are very few results in the three-dimensional case, due to the fact that the governing partial differential equations exhibit the problem of small divisors. In the case that surface tension is an included physical effect, the problem becomes more regular, and there have been several rigorous results in this setting, namely by Reeder and Shinbrot [39], Craig and Nicholls [15] and Groves and Mielke [20].

Our numerical methods for the three-dimensional traveling wave problem are based on the surface spectral method. Calculations can be performed on arbitrary periodic fundamental domains, and we report in this paper on a number of our examples of such. For the most part the three-dimensional numerical calculations in this paper focus on problems of large aspect ratio traveling waves, which can be thought of as nonlinear superpositions of two two-dimensional wavetrains intersecting at an oblique angle. In shallow water, with very oblique intersection, these solutions are compatible with the KP scaling regime, and indeed the solutions that we obtain which are of moderate steepness are comparable to the wave tank experiments and KP modeling of Hammack et al. [22,21]. Our numerical solutions can be extended to very steep hexagonal waves, separating large and very flattened troughs, again exhibiting the robustness of the method (however, see [35–37]).

The difference between the shallow and deep water regimes appears already at ratios of depth to wavelength in the direction of around $h/L \sim 1/10$. Our numerical calculations of large aspect ratio traveling waves have almost a rectangular contour plot, rather than the hexagons seen in the shallow water calculations. Cross-sections of the fluid surface in the direction of propagation do not exhibit the characteristic flattening of troughs and sharpening of crests as in the shallow water case, although there is some asymmetry. Transverse to the direction of motion there is significant broadening, however, giving rise to quite dramatic patterns of rolling waves with crests almost completely aligned orthogonal to the direction of propagation, with crests of one row aligned with the troughs of the adjacent rows, in a periodic array with a long transverse spatial period. These computations are consistent with the deep water traveling wave patterns observed by Henderson and Hammack in the three-dimensional wave tank of the Pritchard Lab at Penn. State University [8]. In case $h = +\infty$ the natural model equation describing this asymptotic regime is that of the two-dimensional cubic nonlinear Schrödinger equation [8], which describes many of the features of these solutions. It does not, however, seem to describe the degree of crest sharpening and trough widening in the direction of propagation that are seen in our numerical solutions.

The organization of this paper is as follows. Section 2 poses the Euler equations for traveling surface water waves and describes the formulation of the problem in terms of Zakharov's canonical conjugate variables as functions on the surface. Here we also give the linearized analysis, and describe the basic points of bifurcation from uniform flow. In Section 3 we describe our principal results for the two-dimensional problem, including the branch of Stokes traveling wavetrains, its solutions of extremal form, and our calculations of secondary bifurcation branches. We also demonstrate the criterium for spectral convergence in this setting. Section 4 is concerned with the three-dimensional bifurcation problem, and a description of the bifurcation surfaces of solutions in a neighborhood of a simple bifurcation point. Finally, Section 5 is given over to a description of our numerical simulations of three-dimensional traveling waves. Our computations include (1) traveling waves whose fundamental domain is nonrectangular, (2) full bifurcation surfaces of traveling waves, giving a continuum of solutions connecting an oblique two-dimensional traveling wave, through a three-dimensional symmetric pattern, and by inference continuing to a two-dimensional oblique pattern traveling in the reflected oblique direction, (3) hexagonal traveling water waves in a shallow water regime, and (4) the analogous large aspect ratio rectangular waves in the deep water case.

Using these methods we have attempted to calculate crescent shaped solutions in the three-dimensional case, with only partial success to date, and we plan to report on this effort in a subsequent publication. Two appendices are included, in which a recurrence formula is given for the Taylor expansion of the Dirichlet–Neumann operator, and the coefficients of the perturbation analysis for bifurcation surfaces are computed.

2. Traveling wave solutions of the water wave problem

We consider the evolution of the free surface of an incompressible, inviscid, irrotational fluid, of constant depth $-h$ where $0 < h \leqslant +\infty$. The infinite depth case $h = +\infty$ is specifically included. The problem that we address in this paper is with zero surface tension, although our numerical method can in principle be extended to include this effect. To fix nomenclature we refer to the water wave problem with an $(n-1)$-dimensional surface and one vertical dimension as the n dimensional problem; this paper discusses both the cases $n = 2$ and 3.

2.1. Surface integral formulation

An ideal fluid inside the domain $S(\eta) = \{(x, y) \in \mathbf{R}^n \mid -h \leqslant y \leqslant \eta(x,t)\}$ with free surface $y = \eta(x,t)$ is described by the system of equations of motion for a fluid under the influence of gravity,

$$\Delta\varphi = 0 \qquad \text{in } -h < y < \eta(x,t), \tag{1a}$$

$$\partial_y\varphi = 0 \qquad \text{at } y = -h, \tag{1b}$$

$$\partial_t\eta + \nabla_x\eta\cdot\nabla_x\varphi - \partial_y\varphi = 0 \qquad \text{at } y = \eta(x,t), \tag{1c}$$

$$\partial_t\varphi + \frac{1}{2}|\nabla\varphi|^2 + g\eta = 0 \qquad \text{at } y = \eta(x,t). \tag{1d}$$

The velocity within the fluid is given by $\mathbf{u} = \nabla\varphi$, and g is the acceleration of gravity. We impose lateral periodic boundary conditions with respect to a lattice $\Gamma \subseteq \mathbf{R}^{n-1}$; in two-dimensions this means that the surface will be parameterized by a fundamental domain that is an interval $\mathbf{T} = [0, L]$, and in three dimensions by a fundamental domain $\mathbf{T} = \mathbf{R}^2/\Gamma$, effectively a parallelogram in $\mathbf{R}^2$. The lattice Γ of spatial periods can be arbitrary, and in particular it need not be rectangular.

Eq. (1) gives the classical formulation of the water wave problem. We will work with an equivalent surface integral formulation of the water wave problem, whose derivation is discussed in detail in Craig and Sulem [18], Nicholls [32], and Nicholls [33]. The origin of this formulation is in Zakharov's observation that the free surface $\eta(x,t)$ and the velocity potential at the free surface $\xi(x,t) = \varphi(x,\eta(x,t),t)$ are canonical conjugate variables for a Hamiltonian form of the water wave problem [54]. Working in these variables, Craig and Sulem introduced the Dirichlet–Neumann operator [18], mapping Dirichlet data for harmonic functions to Neumann data at the free surface, which is defined by,

$$G(\eta)\xi = \big(1 + |\nabla_x\eta|^2\big)^{1/2}\nabla\varphi\cdot N(\eta). \tag{2}$$

Here $N(\eta)$ is the unit exterior normal to the free surface and φ satisfies the boundary value problem

$$\Delta\varphi = 0, \qquad -h < y < \eta(x,t), \tag{3a}$$

$$\partial_y\varphi = 0 \qquad \text{at } y = -h, \tag{3b}$$

$$\varphi\big(x,\eta(x,t)\big) = \xi(x), \tag{3c}$$

$$\varphi(x+\gamma, y, t) = \varphi(x,y,t) \qquad \text{for all } \gamma \in \Gamma. \tag{3d}$$

Expressing the velocity potential and its derivatives on the free surface in terms of ξ and $G(\eta)\xi$, the following set of equations is equivalent to (1):

$$\partial_t\eta = G(\eta)\xi, \tag{4a}$$

$$\partial_t\xi = -g\eta - \frac{1}{2(1+|\nabla_x\eta|^2)}\big[|\nabla_x\xi|^2 - \big(G(\eta)\xi\big)^2 - 2\big(G(\eta)\xi\big)\nabla_x\xi\cdot\nabla_x\eta + |\nabla_x\xi|^2|\nabla_x\eta|^2 - (\nabla_x\xi\cdot\nabla_x\eta)^2\big]. \tag{4b}$$

This is a Hamiltonian system with Hamiltonian

$$H(\eta,\xi) = \frac{1}{2}\int_T \xi G(\eta)\xi + g\eta^2\,\mathrm{d}x,$$

a fact which appears in the bifurcation analysis for traveling waves in several instances. The right-hand side of (4) contains an expression for variations of the Dirichlet integral $\delta_\eta\frac{1}{2}\int_{\mathbf{T}}\xi G(\eta)\xi\,\mathrm{d}x$ with respect to the fluid domain $S(\eta)$, which is a nontrivial computation [18] related to the Hadamard variational formula.

2.2. Traveling wave solutions

We introduce the phase velocity vector $c \in \mathbf{R}^{n-1}$ into Eqs. (4) as a parameter. The details of the derivation of the equations for traveling wave solutions are given in Nicholls [33]; the resulting equations are expressed as

$$F(\eta, \xi, c) = 0,$$

where

$$F_1(\eta, \xi, c) = g\eta + [c \cdot \nabla_x]\xi + \frac{1}{2(1+|\nabla_x \eta|^2)}\big[|\nabla_x \xi|^2 - \big(G(\eta)\xi\big)^2 - 2\big(G(\eta)\xi\big)\nabla_x \xi \cdot \nabla_x \eta + |\nabla_x \xi|^2 |\nabla_x \eta|^2 - (\nabla_x \xi \cdot \nabla_x \eta)^2\big], \tag{5a}$$

$$F_2(\eta, \xi, c) = -[c \cdot \nabla_x]\eta + G(\eta)\xi. \tag{5b}$$

It is natural to use a bifurcation analysis to study solutions of the system $F(\eta, \xi, c) = 0$.

As usual, the first step is to linearize $F = 0$ about the trivial solution $(\eta, \xi, c) = (0, 0, c)$, and to determine the null space of $\partial_u F(0, 0, c)$, where

$$A(c) = \partial_u F(0, 0, c) = \begin{pmatrix} g & c \cdot \nabla_x \\ -c \cdot \nabla_x & G_0 \end{pmatrix}. \tag{6}$$

Under Fourier transform the linear operator $A(c)$ is block diagonal, in 2×2 blocks of the form

$$\hat{A}_k(c) = \begin{pmatrix} g & \mathrm{i}c \cdot k \\ -\mathrm{i}c \cdot k & |k| \tanh(h|k|) \end{pmatrix}, \tag{7}$$

where k are wave numbers in the lattice Γ' conjugate to the lattice Γ of the spatial periods. From this expression, the null space and the bifurcation points are determined by the solutions (c, k) of the dispersion relation

$$\Delta(c, k) = g|k| \tanh\big(h|k|\big) - (c \cdot k)^2 = 0, \tag{8}$$

and the associated null vectors are,

$$\psi_1(c, k) = \begin{pmatrix} c \cdot k \cos(k \cdot x) \\ -g \sin(k \cdot x) \end{pmatrix}, \qquad \psi_2(c, k) = \begin{pmatrix} c \cdot k \sin(k \cdot x) \\ g \cos(k \cdot x) \end{pmatrix}. \tag{9}$$

When $n = 2$, for fixed $k_0 \in \Gamma'$ one can always find a unique (up to sign) phase velocity c satisfying $\Delta(c, k_0) = 0$, and therefore we are in a situation of simple bifurcation. In three dimensions, for a fixed wave vector $k_1 \in \Gamma'$, the equation $\Delta(c, k_1) = 0$ determines two parallel lines of solutions, consisting of a particular solution pair $\pm c_0$, plus all parameters $c \in \mathbf{R}^2$ such that $(c \pm c_0) \perp k_1$. Given any two independent wave vectors $k_1, k_2 \in \Gamma'$ it is always possible to find a phase velocity vector $c^{(0)}$ for which $\Delta(c^{(0)}, k_j) = 0$, $j = 1, 2$ (in fact there are four choices, the intersections of the above pairs of lines). As well it is possible that other $k_j \in \Gamma'$, $k_j \neq \pm k_1, \pm k_2$ will also satisfy $\Delta(c^{(0)}, k_j) = 0$, and one can have multiplicity $p > 2$. For fixed phase velocity $c^{(0)}$, if the wave numbers $\pm k_1, \pm k_2, \ldots, \pm k_p \in \Gamma'$ are those which satisfy $\Delta(c^{(0)}, k_j) = 0$, then $A(c^{(0)})$ has a $2p$ dimensional null space. The situations where $p > 2$ correspond to cases of bifurcation points of higher multiplicity, which are cases of resonance for Eq. (5).

3. Bifurcation curves of two-dimensional gravity waves

The numerical techniques to obtain nontrivial traveling wave solutions of the water wave problem using the surface integral formulation given in Eq. (5) have been described in Nicholls [33]. The procedure can be summarized for the two-dimensional water wave problem; given an initial choice of a wave number k_0 in the conjugate lattice Γ', there is a bifurcation point $c^{(0)}$ (actually two points) which satisifies $\Delta(c^{(0)}, k_0) = 0$. Using a version of the continuation method described in [1] and [24], one follows the bifurcation branch emanating from the trivial solution branch at $c^{(0)}$. The solutions are normalized, in view of the natural S^1 translational symmetry of the problem, by insisting the tangent vector to the initial branch of solutions is given by the solutions of the linear equations

$$\begin{pmatrix} \eta_0(x) \\ \xi_0(x) \end{pmatrix} = r \begin{pmatrix} (c^{(0)} k_0) \cos(k_0 x) \\ -g \sin(k_0 x) \end{pmatrix}. \tag{10}$$

This serves to fix the phase. A numerically converged solution of problem (5) is expected to be quite close to the solution (10), with nearby phase velocity c. This principal bifurcation branch is the numerical approximation of the well-known Stokes wavetrain, computed in the coordinates given by the method. As one moves along the bifurcation branch to higher amplitudes, the solutions of (5) will become "nonlinearizations" of (10), and will develop the characteristic long shallow troughs and sharply peaked crests of the Stokes wavetrain. According to continuation theorems in bifurcation analysis and to the theory of the numerical method, this branch will continue until the point that either the solutions develop singularities or else return to connect to the initial trivial solution branch.

This section of the paper reports on our bifurcation calculations for the Stokes wavetrain and several secondary bifurcation branches. Starting from the point at which a solution branch bifurcates from the trivial solution, we have been able to follow the branch of Stokes waves up very close to the wave of extremal form, with a Lipschitz singularity at their crest with the opening angle of $2\pi/3$ predicted by Stokes. Furthermore, the numerical method seeks secondary bifurcation points along any branch of solutions, and can in principle follow any such solution branches. Without undertaking an exhaustive study of the connected continuum of the multiple secondary bifurcation branches of the Stokes wavetrain, we have pursued several such secondary bifurcation branches up to their own limiting forms, at which some of the crests develop the famous $2\pi/3$ Lipschitz singularity.

The bifurcation problem for two-dimensional traveling gravity water waves has been the object of very much study over many decades, both for the spatially periodic Stokes wavetrain and for solitary waves. Our work on the subject of two-dimensional traveling water waves has several purposes. The original goal was to test our surface integral formulation and the numerical methods in this challenging but quite well understood setting. Because the relevant singular integrals are well approximated by Fourier transform based methods, the surface integral formulation has essentially the computational and memory storage costs of a one-dimensional problem in spatial resolution, and furthermore the approach is able to take advantage of the spectral character of the computation and the efficiency of the fast Fourier transform. These computations are able to include many Fourier modes and encompass a full de-aliasing procedure. With our method, we are able to make explicit estimates of the rate of convergence of our solutions to solutions of the Euler flow. Our computations allow us to obtain details of their secondary bifurcations and their approach to the limiting Stokes waves of extremal form. A fact to emphasize is that the numerical method is not one that is designed for nor particularly specialized to resolve Lipschitz singularities, despite the theoretical fact [11] that the Dirichlet–Neumann operator depends analytically upon the function η in the Lipschitz topology. It surprized us to some extent that the computations that we undertook were able to resolve the Stokes waves of limiting form to a high degree, and we take this as a sign of the robustness of the approach.

3.1. The Stokes wavetrain

Our first computation is of the bifurcation branch B_1, a branch of solutions originating on the set of trivial solutions from the bifurcation point $c^{(0)}$, the solution family described by Stokes. We set $g = 1$, and we initially chose $h = 0.1$, and $L = 1$ to obtain a realistic aspect ratio for the fluid domain. With these choices, the bifurcation point for the solutions with fundamental period L is given by

$$c^{(0)} = \sqrt{\frac{\tanh((0.1)2\pi)}{2\pi}} \sim 0.297712. \tag{11}$$

There is an upper bound [17] for the amplitude $a = |\eta|_{L^\infty}$ of a solution in terms of the phase velocity, given by

$$a \leqslant \frac{c^2}{2g} = a_\ell(c), \tag{12}$$

which we note is independent of the fluid depth h. Equality is achieved only for the wave of extremal form with the Lipschitz crest. In Fig. 1 we have a plot of the bifurcation branch in terms of the norm of solution $a = |\eta|_{L^\infty}$ and the phase velocity c. For reference, the plot also includes the graph of the function $a_\ell(c)$ describing the phase velocity of solutions of extremal form. The intersection of these two curves gives the values of the amplitude a^{extremal} and phase velocity c^{extremal} of the solution of extremal form. Solution profiles for the wave of extremal form of the bifurcation branches B_2 and B_{21} are given in the two graphs in Fig. 2.

The principal bifurcation branches B_1 and B_2 exhibit the Tanaka phenomenon of a turning point at the fastest traveling wave of indicated period, which occurs high on the solution branch. For comparison, the wave of extremal form on branch B_1 has a numerically computed velocity $c^{\text{extremal}} = 0.334794$ and amplitude $|\eta|_{L^\infty} = a^{\text{extremal}} = 0.56009h$, while the fastest wave has velocity $c = 0.334983$ and amplitude $|\eta|_{L^\infty} = 0.55072h$. We remark that the difference in height and velocity between the tallest and the fastest Stokes waves is much more pronounced for periodic traveling waves than for the solitary wave [23,49], and periodic Stokes wavetrains can apparently be as much as 0.2% faster at the solution of maximal phase velocity, as the solution of extremal form.

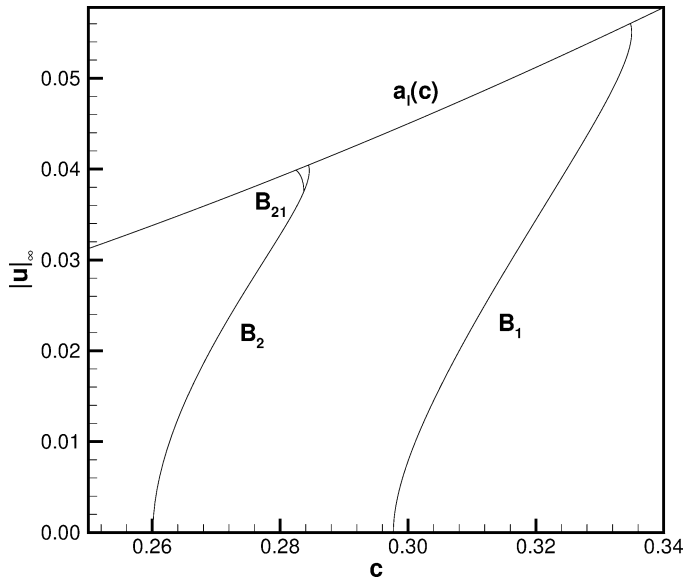

Fig. 1. Plot of the bifurcation curves B_1, B_2 and the secondary bifurcation curve B_{21} in the phase speed-amplitude plane ($a = |u|_\infty, c$). We include the upper bound $a_\ell(c)$. ($L = 1$, $h = 1/10$ and $g = 1$).

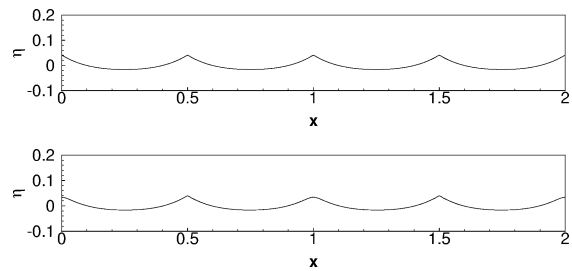

Fig. 2. Plots of the extremal waves on branches B_2 (top, $c^{\text{extremal}} = 0.334861$), and B_{21} (bottom, $c^{\text{extremal}} = 0.334983$); $h = 1/10$.

The upper bound $a_\ell(c)$ for the occurrence of Lipschitz singularities does not specify $|\eta|_{L^\infty}$ for solutions of extremal form, only a relationship between the amplitude and the phase velocity of such. Producing similar solution branches of two-dimensional Stokes wavetrains with varying fundamental period L, we explored the behavior of the amplitude (respectively, the phase velocity) of the waves of extremal form on the principal bifurcation branch, for periods L between $L = 1$ and $L = 160$. A graph of the extremal amplitude $a^{\text{extremal}}(L)$ as a function of fundamental period L is given in Fig. 3. Note that the estimates in [17] imply that a priori the extremal amplitude satisfies $a^{\text{extremal}} \leqslant h$, while for solitary waves they also imply the lower bound $h/2 \leqslant a^{\text{extremal}}$.

3.2. Subharmonic secondary bifurcations

A second goal of the two-dimensional calculations is to study to some extent the secondary bifurcations of the problem of two-dimensional traveling water waves. Seeking subharmonic secondary bifurcation points along given branches of solutions, we produce a variety of bifurcation curves, whose extremal solutions are Lipschitz-singular crested waves of extremal form with different character, and in particular with different phase velocities. The point of intersection of each bifurcation branch and the extremal parabola $a_\ell(c)$ from (12) changes with depth h, spatial period L and acceleration of gravity g, with one scaling relation between them, as we have described in the previous paragraph. We show that for fixed g, h and L this point of intersection varies from one bifurcation branch to another, and that details of the patterns of crests differ. In particular, we have calculated a branch of solutions of period $2L$ which bifurcates from the branch of Stokes wavetrains of period L. Denoting the simple bifurcation branch for spatial period L by $B_1(L)$, that for period $2L$ by $B_1(2L)$ and the secondary bifurcation branch stemming from $B_1(L)$ at the point $(c_1, a_1) = (0.283705, 0.037527)$ by $B_{21}(L)$, we have calculated the phase velocities of the extremal waves of the branches $B_1(L)$ and $B_{21}(L)$ to be $c_1^{\text{extremal}}(L) = 0.284448$ and $c_2^{\text{extremal}}(L) = 0.282515$, respectively.

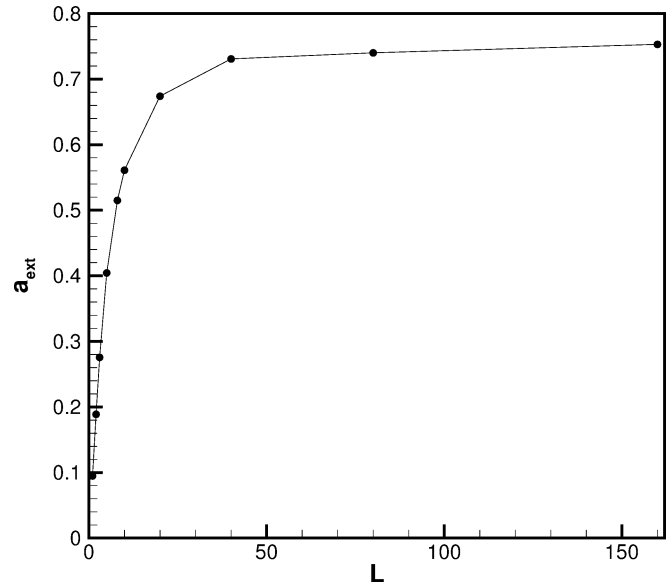

Fig. 3. Graph of $a^{\text{extremal}}(L)$ as a function of wavelength L.

Table 1
The computed phase velocity and amplitude of the extremal wave at the limit of several different bifurcation branches. The error is defined by comparison of $c_j^{\text{extremal}}(nL)$ and $a_j^{\text{extremal}}(nL)$ with the relation (12): error = $(c_j^{\text{extremal}}(nL))^2/2 - a_j^{\text{extremal}}(nL)$

Branch	Computed phase velocity	Computed amplitude	Error
$B_1(L)$	$c_1^{\text{extremal}}(L) = 0.284448$	$a_1^{\text{extremal}}(L) = 0.040426$	2.933×10^{-5}
$B_1(2L)$	$c_1^{\text{extremal}}(2L) = 0.334794$	$a_1^{\text{extremal}}(2L) = 0.056009$	3.451×10^{-5}
$B_{21}(L)$	$c_2^{\text{extremal}}(L) = 0.282515$	$a_2^{\text{extremal}}(L) = 0.039868$	3.936×10^{-5}

Principal features to notice are that (i) the extremal solution of branch $B_{21}(L)$ has alternately singular and regular crests, the former of slightly higher amplitude than the latter, and (ii) that $\partial_a c(a) < 0$ along the entire secondary branch $B_{21}(L)$, which is to say that the solution is quite markedly slowing as it increases in amplitude from the secondary bifurcation point.

In particular this solution branch does not experience a sequence of oscillations in the sign of the derivative of the phase velocity as a increases, something that is generally indicative of subsequent further bifurcation points and exchanges of stability. This is unlike the primary branch, for which $\partial_a c(a) > 0$ from the initial bifurcation point at the quiescent state all the way up to a very high turning point near to the Stokes waves of extremal form.

3.3. Harmonic and superharmonic bifurcation

A third goal is to explicitly seek harmonic and superharmonic bifurcations from the principal branches $B_1(L)$. Fixing a depth h and spatial period L, we systematically computed the Jacobian of the mapping F along the computed solution branches $B_1(L)$, with L restricted explicitly to be the maximal allowed spatial period for the computation. As we use a continuation method and a Newton scheme, this information is a natural output from the numerical computations. As long as the number of Taylor series terms in the approximation for the operator $G(\eta)$ was sufficiently large ($m \geqslant 3$ is appropriate), the eigenvalues of the Jacobian appeared to remain bounded away from zero along the entire branch, including after the turning of the solution curve at the fastest wave. This is consistent with the numerical results of [9,10]. Additionally, the main result of Buffoni, Dancer and Toland [6] is that the Morse index of solutions along the principal bifurcation branch diverges as the branch approaches the solution of extremal form. This is due either to the existence of an infinite number of secondary harmonic or superharmonic bifurcation points along the branch, or else to an infinite number of turning points. Our numerical evidence is for the latter case, rather than the former.

3.4. The numerical method and a convergence study

This section is devoted to a description of the numerical method that we use in our experiments, and we also present the results of a convergence study for two-dimensional traveling waves. In brief, the numerical method is a predictor-corrector continuation technique [1] applied to the equations

$$F_{N,m}(u_{N,m}, c_{N,m}) = 0,$$

where in these equations $c_{N,m}$ is an approximation to the wave speed, and $u_{N,m} = (\eta_{N,m}, \xi_{N,m})$ is a vector of approximations to the wave profile, η, and surface velocity potential, ξ, at the N equally spaced collocation points on the interval $[0, L]$. The function $F_{N,m} : \mathbf{R}^{2N+1} \to \mathbf{R}^{2N}$ is derived from the F presented at the beginning of Section 2.2, cf. (5), by a Fourier collocation procedure [7]. This takes advantage of accurate approximations of the Dirichlet–Neumann operator $G(\eta)$ using the fast Fourier transform. The operator $G(\eta)$ varyies analytically in $\eta(x) \in \mathrm{Lip}(\mathbf{R}^{n-1})$ as a mapping of function spaces $H^1(\mathbf{T}) \to L^2(\mathbf{T})$, this is described in [11,16,15], and therefore it can be given by a convergent Taylor series.

$$G(\eta) = \sum_{j=0}^{\infty} G_j(\eta), \tag{13}$$

where the Taylor polynomials $G_j(\eta)$ are operators which are homogeneous of degree j in η. It furthermore turns out that these Taylor polynomials can be computed recursively, in terms of concatenations of multiplication by powers of $\eta(x)$, and the Fourier multipliers $D = -\mathrm{i}\partial_x$ and $\mathrm{i}\tanh(h|D|)$. Because of this form of the expansion, it is useful to represent functions on the periodic fundamental domain $\mathbf{T} = \mathbf{R}^{n-1}/\Gamma$ in terms of their Fourier series expansion $\xi(x) = \sum_{k\in\Gamma'} \hat{\xi}(k)\mathrm{e}^{\mathrm{i}k\cdot x}$, where Γ' is the dual lattice to Γ.

Our numerical approximation of $G(\eta)$ consists of the Taylor series of $G(\eta)$ about the point $\eta = 0$, truncated at order $m \geqslant 0$ in order to retain m terms in the Taylor expansion of the Dirichlet–Neumann operator, cf. (37):

$$G^{(m)}(\eta) = \sum_{j=0}^{m} G_j(\eta). \tag{14}$$

The structure of the recursion formula implies that the action of the Taylor polynomials $G(\eta)\xi$ in the approximation (14) can be calculated through alternate operations of multiplication and Fourier multiplication (multiplication operations on the Fourier series). This method was implemented in [18,32,33], and in the latter reference it is described in detail.

The computations that appear in this article have been performed using an innovation on this spectral approach to approximate $G(\eta)$. The Dirichlet–Neumann operator is self-adjoint on $L^2(\mathbf{T})$, so that the adjoint formula to that appearing in [18,32] is equally valid. The resulting recursion formulae allows one to compute the approximations $G^{(m)}(\eta)\xi$ with vector operations on $\xi(x)$, instead of having to store the matrix components of the approximation of the full operators $G_j(\eta)$. The procedure allows for faster calculations which in addition allows for higher accuracy, as one can include more components in the approximations of $\eta(x)$ and $\xi(x)$. In principle, the computation of $G^{(m)}(\eta)\xi(x)$ using N Fourier modes to approximate $\eta(x)$ and $\xi(x)$ with full de-aliasing takes $Cm^2N\log(mN)$ operations. In practice, we use full de-aliasing with $N \sim 256^{n-1}$ and $m \sim 5$ when calculating $G^{(m)}(\eta)\xi(x)$. Further details of this surface spectral method are given in [33], and the details of this new form of a recursion formula for $G(\eta)$ are given in Appendix A.

In order to test the robustness of our numerical scheme we have designed the following convergence study. We computed two-dimensional traveling wave solutions from the trivial branch to three points (denoted (A), (B), and (C)) along the branch B_1 at roughly one-third, two-thirds, and nine-tenths of the way to the Stokes critical solution, see Fig. 4. In order to uniformly compare solutions corresponding to different values of the discretization parameters m and N, all adaptive step-sizing [1,33] is suppressed as these features are extremely sensitive to changes in parameter. While this is not the procedure used to achieve the numerical results presented above, it does present a more stringent challenge for the numerical method. In particular, smaller step sizes are no longer allowed in difficult portions of the bifurcation curve.

Given the spectral nature of our discretization scheme and the analytic behavior of the Dirichlet–Neumann operator, if u is the exact solution one should expect the following estimate on differences in L^∞-norms to be true

$$\big||u_{N,m}|_{L^\infty} - |u|_{L^\infty}\big| \leqslant C\,\mathrm{e}^{\alpha N}\,\mathrm{e}^{\beta m} \tag{15}$$

for $\alpha, \beta < 0$. While this precise relationship cannot be tested directly as the exact solution is unknown, we decided to test the following relationship comparing approximate solutions against a "well-resolved" solution corresponding to a computation with $N = 96$ and $m = 5$:

$$\varepsilon_n(N,m) \equiv \big||u_{N,m}|_{L^\infty} - |u_{96,5}|_{L^\infty}\big| \leqslant C\,\mathrm{e}^{\alpha_n N}\,\mathrm{e}^{\beta_n m} \tag{16}$$

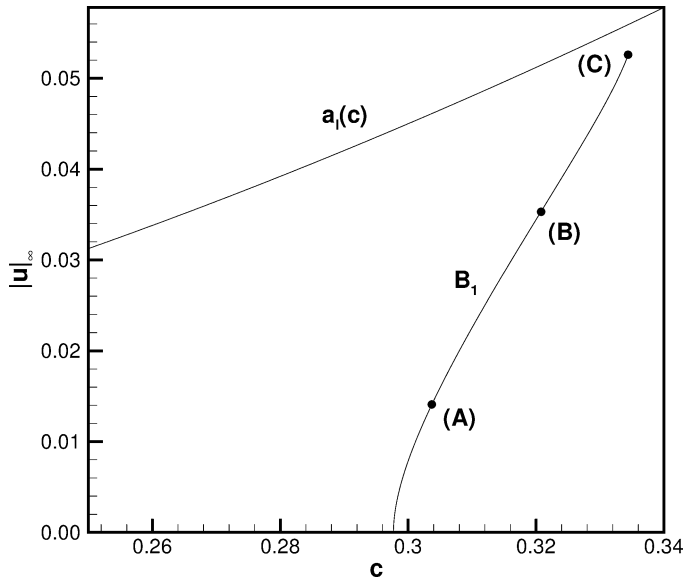

Fig. 4. Test points (A), (B), (C) along the bifurcation branch B_1.

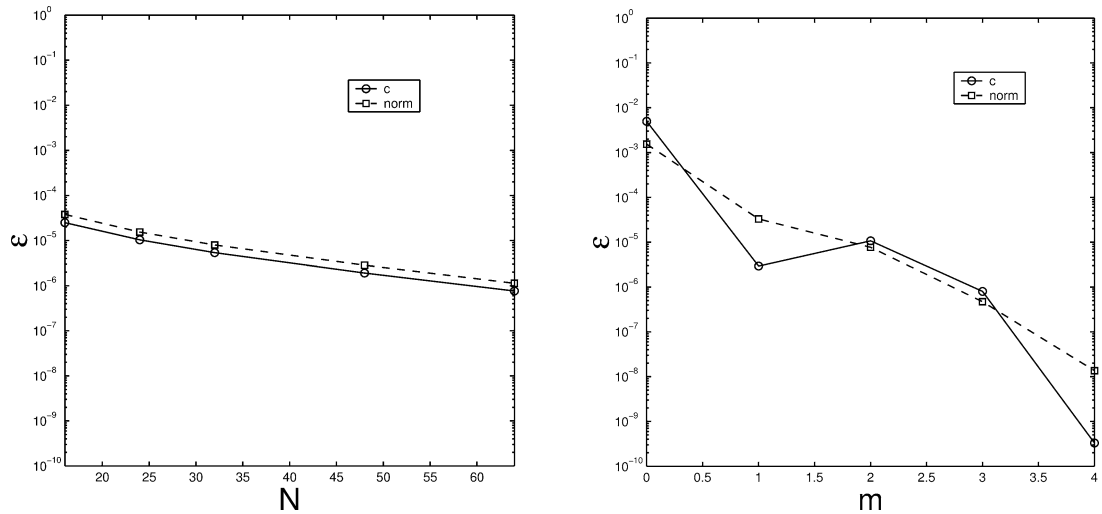

Fig. 5. Log-linear plots of $\varepsilon(N,3)$ (left) and $\varepsilon(64,m)$ (right) for the point (A) along the branch B_1.

for $N < 96$ and $m < 5$. One can also measure the difference between an approximate speed and a well-resolved calculation of the speed, i.e., test the relationship

$$\varepsilon_c(N,m) \equiv |c_{N,m} - c_{96,5}| \leqslant C\, \mathrm{e}^{\alpha_c N}\, \mathrm{e}^{\beta_c m} \tag{17}$$

for $N < 96$ and $m < 5$. Computations of ε_n and ε_c were carried out for various values of N and m and the results are presented in Fig. 5 for point (A), Fig. 6 for point (B), and Fig. 7 for point (C). In each figure one sees on the left $\varepsilon(N,3)$ for $N = 16, 24, 32, 48, 64$, while on the right we display $\varepsilon(64,m)$ for $m = 0, 1, 2, 3, 4$. Notice that all figures use the same vertical range so that a direct comparison of the absolute errors can be made: the errors obtainable at point (A) are significantly less than those achievable at point (B) which, in turn, are much smaller than those made at point (C).

These results are further summarized in Tables 2 and 3. For the data presented in Table 2, m was held fixed at 3 and N was allowed to vary from 16 to 64, and then a least squares fit was used to approximate α_n and α_c. We note that in each case the exponent is negative (indicating convergence), however, as the final point is moved closer to the critical curve the magnitude of the α's, and thus the rate of convergence, decreases. For the data presented in Table 3, N was held fixed at 64 and m was

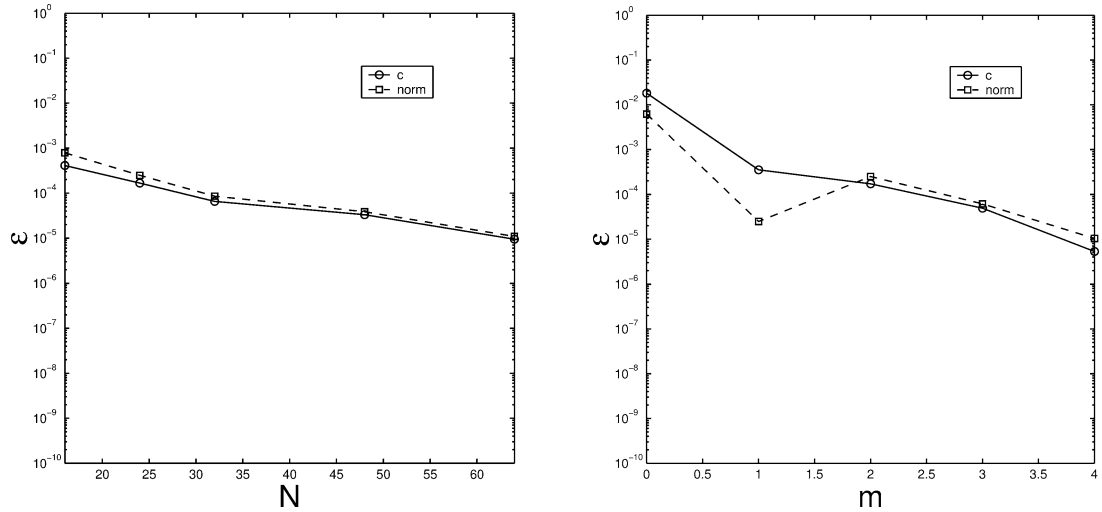

Fig. 6. Log-linear plots of $\varepsilon(N,3)$ (left) and $\varepsilon(64,m)$ (right) for the point (B) along the branch B_1.

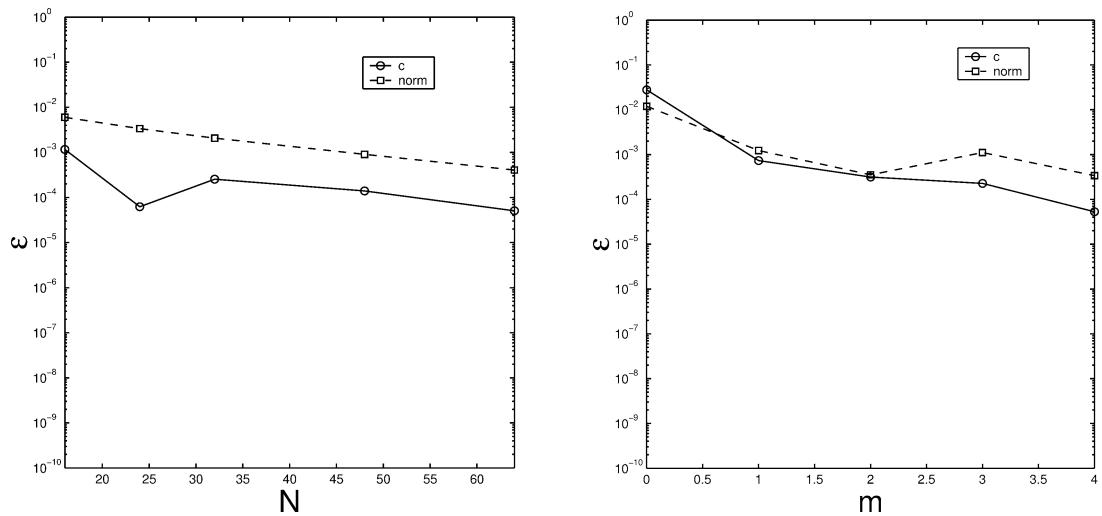

Fig. 7. Log-linear plots of $\varepsilon(N,3)$ (left) and $\varepsilon(64,m)$ (right) for the point (C) along the branch B_1.

Table 2
Spectral convergence constants with fixed $m = 3$ for the norm test (16) and the wave speed test (17) where N was allowed to range from $N = 16, 24, 32, 48, 64$

Test point	α_n	α_c
(A)	–0.0710183	–0.0706612
(B)	–0.0839919	–0.0743555
(C)	–0.0550863	–0.0433343

allowed to vary from 0 to 4, and then a least squares fit was used to approximate β_n and β_c. Again, in each case the exponent is negative, however, as the final point is moved closer to the critical curve the magnitude of the β's decreases.

Table 3
Spectral convergence constants with fixed $N = 64$ for the norm test (16) and the wave speed test (17) where m was allowed to range from $m = 0, 1, 2, 3, 4$

Test point	β_n	β_c
(A)	–2.75245	–3.43524
(B)	–1.18788	–1.82533
(C)	–0.722927	–1.37035

4. Three-dimensional bifurcation surfaces

Our next consideration is the problem of three-dimensional surface water waves, for which the free surface is doubly periodic in the horizontal variables $x = (x_1, x_2) \in \mathbf{R}^2$. The question of traveling waves is again a bifurcation problem, where one seeks a solution (η, ξ) to Eq. (5), along with a phase velocity vector $c = (c_1, c_2)$. One of the points that we are making is that this bifurcation problem possesses a two-dimensional parameter space, and this has the consequence that the interesting bifurcation points occur for values of c for which there are at least two linearly independent solutions of the linearized problem (6). A simple bifurcation is one in which the multiplicity of solutions to the linearized problem is exactly two. Solutions to the nonlinear problem occur in the typical form of bifurcation branches which are two-dimensional surfaces rather than one-dimensional curves, and the structure of the set of solutions is more interesting than for problems with one bifurcation parameter. For numerical continuation methods this poses a difficulty in that, unlike arc-length parametrization for curves, surfaces have no canonical method of parametrization. For the numerical results in this paper, we either map out portions of a bifurcation surface in (essentially) geodesic polar cordinates, or else we choose to follow certain distinguished curves in the bifurcation surfaces under consideration, using the more standard continuation method for bifurcation curves. At bifurcation points with higher number of solutions to the linearized problem, there is a further theory of multiplicity of solution branches which is described in [15] (at least in the case that surface tension is included in the problem) which is based on the Hamiltonian form of the water wave equations.

For the three-dimensional problem, solutions of (5) are defined on a periodic fundamental domain $\mathbf{T} = \mathbf{R}^2(x)/\Gamma$, where Γ is a lattice of translations of $\mathbf{R}^2(x)$. This is to say that solutions $(\eta(x), \xi(x))$ are taken to satisfy the condition that $(\eta(x+\gamma), \xi(x+\gamma)) = (\eta(x), \xi(x))$ for all translations $\gamma \in \Gamma$, and this sets the boundary conditions on the lateral sides of the fluid domain. The fundamental domain $\mathbf{T}$ need not be rectangular, indeed our numerical method allows for any lattice Γ, and this is important when considering solutions which have special resonance relations, or with particular symmetries, such as symmetric diamonds. Along with this flexibility of choice of fundamental domain, the phase velocity vector c is part of the solution, and it must be kept in mind that it cannot be assumed to have any a priori geometrical relationship with the lattice Γ, except in particularly symmetric situations. In addition, the momentum of the solutions, which is given by the expression $I = (I_1, I_2)$, where

$$I_1(\eta, \xi) = \int_{\mathbf{T}} \xi \, \partial_{x_1} \eta \, \mathrm{d}x, \qquad I_2(\eta, \xi) = \int_{\mathbf{T}} \xi \, \partial_{x_2} \eta \, \mathrm{d}x, \tag{18}$$

need not be parallel to the phase velocity c of that solution, and again it cannot be assumed to have an a priori relationship with Γ.

The degree of nonlinearity in the resulting wave field can be gauged in terms of the maximal slope $|\eta|_{\mathrm{Lip}}$, and as in the two-dimensional case the principal nonlinear effects include the change in phase velocity as a function of amplitude, and the appearance of sharper crests and wider broadened troughs. These nonlinear features are however markedly different in the two cases of deep water and shallow water short-crested waves. In shallow water, the solutions with relatively large aspect ratio fundamental domains tend to form hexagonal structures, that is to say they have a wide and flat trough which is effectively surrounded by a six sided ridge. The two highest sides of the ridge are oriented perpendicularly to the phase velocity vector c, and are the result of the nonlinear superposition of two two-dimensional wavetrains at an oblique angle. In deep water, the large flat trough is no longer present, and the traveling wavetrains take the form of an alternating series of rolls oriented in the direction of motion c. Even for nonlinear wavetrains of considerable steepness, the profile of the solution in a plane aligned with the direction of motion is not far from sinusoidal. However in directions orthogonal to c, these solutions have very long, flattened profiles, either along crest or trough, with periodically spaced transition regions between the two which are of order one. The description of the difference between shallow water and deep water three-dimensional traveling wavetrains is the topic of the paper [34] and is one of the principal topics of the present article. As well, it is one of the subjects of focus of our current research program [8], which gives a number of related experimental, numerical and theoretical results on its web page.

The main point that we would like to make in this section is that the existence of these traveling waves is not an isolated phenomenon, but rather (1) the family of short-crested waves is connected continuously to obliquely traveling Stokes waves, through a two-dimensional bifurcation surface, (2) there exist families of solutions of the water wave problem which vary continuously from short-crested waves to large aspect ratio hexagonal patterns as one varies the depth of the fluid region, and (3) at a point c_0 of simple bifurcation from the trivial solution $(\eta, \xi) = 0$ there are four solution surfaces which intersect at c_0 in a certain canonical pattern, the trivial branch $c = 0$ and three other nontrivial solution branches.

The paper [30] poses a question for the three-dimensional water wave problem which can be restated as to whether traveling waves are uniquely specified by the fundamental domain $\mathbf{T}$ and the wave height, or if not, at least are solutions with these specifications isolated. The answer is that this is not so, that in fact solutions do not occur in one-dimensional bifurcation curves but rather in two-dimensional bifurcation surfaces, and in general will never be isolated.

Consider a fundamental domain $\mathbf{T} \subseteq \mathbf{R}^2(x)$, in nonresonant cases where there are only two wave vectors k_1, k_2 with coincident phase velocity. Locally in a neighborhood of a simple bifurcation point c_0, the solution set consists of the trivial branch, two families of two-dimensional Stokes wavetrain solutions whose basic wave vectors are respectively k_1 and k_2, and a third bifurcation surface consisting of fully three-dimensional traveling wave solutions. This is the analog of simple bifurcations with one parameter, where in a neighborhood of a bifurcation point there are two families of bifurcation curves; these are often the trivial branch and the nontrivial one-dimensional bifurcation branch. We find that a sufficient set of parameters for a local description of the set of fully three-dimensional traveling wave solutions consists of the two components of the momentum, at least for small amplitudes. This situation is the analog of simple bifurcation in one parameter problems. It could also happen that the momentum alone does not supply sufficiently many parameters to locally uniquely describe the solution set; this will happen in neighborhoods of intersections of several of the bifurcation surfaces of this picture.

4.1. Simple bifurcation theory with multiple parameters

In this section we will describe a multiple parameter bifurcation analysis of the system (5), outlining the method for the case of simple bifurcation with multiple parameters. The system of Eqs. (5) is written in the abstract form

$$F(\eta, \xi; c) = \begin{pmatrix} F_1(\eta, \xi, c) \\ F_2(\eta, \xi, c) \end{pmatrix} = 0, \tag{19}$$

where $F(\eta, \xi; c)$ is the nonlinear functional which describes the right-hand side of (5). Its linearization about the quiescent solution $(\eta, \xi) = 0$ is given in (6). When the linearized equation has two or more linearly independent solutions respecting the periods of the fundamental domain $\mathbf{T}$, then the phase velocity c is a bifurcation point. The null space is always even dimensional, for reasons having to do with the Hamiltonian structure of the problem, we will take its dimension to be $2p$. Given a wave vector k and a phase velocity c satisfying the dispersion relation

$$\Delta(k, c) = g|k| \tanh\big(h|k|\big) - (c \cdot k)^2 = 0, \tag{20}$$

the resulting null space contains the two eigenfunctions $\psi_1(c, k)$, $\psi_2(c, k)$ in (9). To start the discussion of bifurcation phenomena, suppose that $p = 1$; then the bifurcation branch of nontrivial solutions consists of two-dimensional Stokes waves, which are constant in some horizontal direction. Such bifurcation points in $n \geqslant 3$ are never isolated, since the dispersion relation (20) depends upon c through the quantity $(c \cdot k)^2$, and for fixed k this defines a line of bifurcation points in the parameter space $\mathbf{R}^2(c)$ (actually two lines, one for each direction of propagation). For two independent wave vectors k_1 and k_2 (and choosing the directions of propagation) the two resulting lines meet in a point $c^{(0)}$ at which the linearized equation (6) has at least a four-dimensional solution space, containing $\psi_j(c^{(0)}, k_1)$, $\psi_j(c^{(0)}, k_2)$, $j = 1, 2$, of (9). If $p = 2$ this constitutes the situation of simple bifurcation. It also could be the case that $p \geqslant 3$, meaning that there are additional linearly independent solutions, associated to $\psi_j(c^{(0)}, k)$ for the other possible solutions k of $\Delta(c^{(0)}, k) = 0$. In the neighborhood of these points the bifurcation analysis is more difficult, and of course more interesting.

Let us take up the case $p = 2$, which describes the simplest three-dimensional short-crested wave patterns. The system of Eqs. (5) is split by projection P onto the range of the linearized operator in (6), and its complementary projection Q, which by abuse of notation can be considered the projection onto the linear span

$$X_1 = \operatorname{span}\big(\psi_1\big(c^{(0)}, k_1\big), \psi_2\big(c^{(0)}, k_1\big), \psi_1\big(c^{(0)}, k_2\big), \psi_2\big(c^{(0)}, k_2\big)\big)$$

of the solutions of the homogeneous linear equation (6). The system of Eqs. (5) is equivalent to

$$QF = 0 \quad \text{and} \quad PF = 0. \tag{21}$$

The first of these is the bifurcation equation, essentially the compatibility condition for the solution of (5). The Lyapunov–Schmidt decomposition consists in writing all vector functions $u = (\eta, \xi)^{\mathrm{T}} = v + w$, where $v = Qv \in X_1$ is in the null space, and $w = (I - Q)u$ is the remainder, and one expects that the second equation

$$PF\big(v + w(v, c), c\big) = 0 \tag{22}$$

is solvable for $w = w(v, c)$, at least locally near the bifurcation point. In reality, for the case of the water wave problem without surface tension this is a small divisor problem, and there are considerable analytic issues that arise (these are avoided with surface tension [15]). These issues aside, under the hypothesis that $p < +\infty$, this procedure in principle reduces the problem to the Q-equation, which is a finite dimensional mapping from $X_1 \times \mathbf{R}^{2p}(c) \to Y_1,\ \mathbf{R}^{2p}(v) \times \mathbf{R}^2(c) \to \mathbf{R}^{2p}$. We note that the dimensions of the null space X_1 and the co-range Y_1 coincide, due to the structure of the original equations (5).

Under the assumption that we have $p = 2$, the minimal interesting dimension, all the solutions of the linear equation (6) are given by

$$v = a_1\psi_1\big(c^{(0)}, k_1\big) + b_1\psi_2\big(c^{(0)}, k_1\big) + a_2\psi_1\big(c^{(0)}, k_2\big) + b_2\psi_2\big(c^{(0)}, k_2\big), \tag{23}$$

for $(a_1, a_2, b_1, b_2) \in \mathbf{R}^4(v)$. There is however a redundancy in the bifurcation problem (21) having to do with the invariance of the equations under translations in the plane $\mathbf{R}^2(x)$. Because of the periodic boundary conditions this is a two-torus symmetry, given explicitly by the transformation $T_\alpha(x_1, x_2) = (x_1 + \alpha_1, x_2 + \alpha_2)$ substituted into (23). The redundancy can be eliminated by the normalization $b_1 = b_2 = 0$, which is tantamount to the restriction to solution components η which are even and ξ which are odd with respect to the two reflections $R_1 : (k_1 \cdot x) \to -(k_1 \cdot x), (k_2 \cdot x) \to (k_2 \cdot x)$ and $R_2 : (k_1 \cdot x) \to (k_1 \cdot x), (k_2 \cdot x) \to -(k_2 \cdot x)$. This property under reflection is preserved by the nonlinear mappings QF and PF, and therefore the bifurcation problem (21) can be reduced to the problem of finding zeroes of the mapping $QF : \mathbf{R}^{2(p-1)}(v) \times \mathbf{R}^2(c) \to \mathbf{R}^{2(p-1)}$. The same redundancy of a two-torus symmetry from the translational invariance of the equations occurs for any dimension of the null space $2p$.

Returning to the case $p = 2$, we consider the bifurcation equation (21), denoting $QF(v + w(v, c)) = f(a, c)$ a vector function of four independent variables, $a \in \mathbf{R}^2(a)$ and $c \in \mathbf{R}^2(c)$. Inspecting the bifurcation point $(0, c^{(0)})$, we find that $f(a, c)$ satisfies

$$\begin{aligned} &f(0, c) = 0, \\ &\partial_a f(0, c^{(0)}) = 0, \\ &\partial_c^\gamma f(0, c) = 0 \quad \text{for all } \gamma \geqslant 1. \end{aligned}$$

Expressing f in the basis given in (23), the Taylor series expansion about the bifurcation point $(a, c) = (0, c^{(0)})$ has the form

$$f(a, c) = \begin{pmatrix} \left(\frac{2g(c^{(0)} \cdot k_1)}{(c^{(0)} \cdot k_1)^2 + g^2}\right) a_1 (c^{(0)} - c) \cdot k_1 \\ \left(\frac{2g(c^{(0)} \cdot k_2)}{(c^{(0)} \cdot k_2)^2 + g^2}\right) a_2 (c^{(0)} - c) \cdot k_2 \end{pmatrix} + \mathcal{O}\big(|a|^2\big) + \mathcal{O}\big(\big|c^{(0)} - c\big|^2 |a|\big). \tag{24}$$

Near the bifurcation point $(a, c) = (0, c^{(0)})$ the set of solutions to (5) does not locally form a manifold, but rather a transversal intersection of several smooth solution surfaces S_j, possessing distinct tangent planes $T(S_j)$ at the bifurcation point. By inspection of the set of solutions of $f(a, c) = 0$ in a neighborhood of the bifurcation point $(0, c^{(0)})$, we have the following local description of the solution set of (5).

Theorem 4.1. *Consider solutions of* (5) *with periodic fundamental domain* **T**. *Assume that*

(1) *the point* $(v, c) = (0, c^{(0)})$ *is a bifurcation point, and*
(2) *the space* X_1 *of linear solutions of* (6) *is four dimensional* (*that is,* $p = 2$).

Then in a neighborhood of the bifurcation point $(0, c^{(0)})$ *the set of solutions can be described by four two-dimensional analytic surfaces* $S_0,\ S_1,\ S_2,\ S_3$ *within the four-dimensional space* $\mathbf{R}^2(a) \times \mathbf{R}^2(c)$. *At the bifurcation point the tangent planes* $T(S_j),\ j = 1, 2, 3, 4$ *to these surfaces do not coincide, and are such that* $T(S_0) \cap T(S_3)$ *and* $T(S_1) \cap T(S_2)$ *are both points, and* $T(S_0) \cap T(S_1),\ T(S_0) \cap T(S_2),\ T(S_1) \cap T(S_3)$ *and* $T(S_2) \cap T(S_3)$ *are lines.*

The surface $S_0 = (0, c)$ for $c \in \mathbf{R}^2(c)$ is the trivial branch of solutions, with $T(S_0) = (0, c)$ as well. The surface S_1 has tangent plane $T(S_1) = \{a_2 = 0, (c^{(0)} - c) \cdot k_1 = 0\}$, and it is formed of a branch of two-dimensional Stokes periodic traveling wave solutions with phase velocity normal to the crest $s = c \cdot k_1$, with an arbitrary phase velocity component tangential to the

crest. The surface S_2 is similar; $T(S_2) = \{a_1 = 0, (c^{(0)} - c) \cdot k_2 = 0\}$, and S_2 consists of the two-dimensional Stokes waves with phase velocity $s = c \cdot k_2$ normal to the crest, and arbitrary phase velocity component tangential to the crest.

Finally, the truly three-dimensional short-crested waves form the surface S_3. The tangent space is $T(S_3) = \{(c^{(0)} - c) \cdot k_1 = 0, (c^{(0)} - c) \cdot k_2 = 0\}$, and the surface is parametrized by the two amplitudes $(a_1, a_2) \in \mathbf{R}^2(a)$ of the null space. This surface intersects the family S_0 of trivial solutions in the point $(0, c^{(0)})$ alone. These solution families unfortunately lie naturally within a four-dimensional space $\mathbf{R}^2(a) \times \mathbf{R}^2(c)$ and therefore are less easily visualized than bifurcation curves. Nonetheless one can see that S_3 provides a connecting surface of three-dimensional short-crested waves which intersect both the surfaces of two-dimensional Stokes waves S_1 and S_2 in one-dimensional curves.

This result is comparable to the main theorem of the paper [15], where the resonant case $p > 2$ is also considered. In such resonant situations, one is guaranteed at least $p-1$ distinct solutions for every choice of the horizontal momentum, by a theorem that is analogous to the resonant Lyapunov center theorem. The solutions are thus parametrized by their momentum, in at least $p-1$ many solution families, although the smoothness of these families is not implied, and in general does not hold true.

4.2. Perturbation analysis of nonresonant short-crested waves

It is possible to determine the nature of the bifurcation surfaces S_1, S_2 and particularly S_3 to higher order, using a formal perturbation calculation. Since S_1 and S_2 consist of two-dimensional Stokes waves with phase velocity effectively in the directions of k_1 and k_2, these are well characterized by two-dimensional perturbation analysis (starting with Stokes himself [45]) and the real interest is in the description of S_3. The Ansatz for our perturbation analysis has the following form,

$$\begin{pmatrix} \eta \\ \xi \end{pmatrix} = \varepsilon \begin{pmatrix} \eta^{(1)} \\ \xi^{(1)} \end{pmatrix} + \varepsilon^2 \begin{pmatrix} \eta^{(2)} \\ \xi^{(2)} \end{pmatrix} + \varepsilon^3 \begin{pmatrix} \eta^{(3)} \\ \xi^{(3)} \end{pmatrix} + \mathcal{O}\big(\varepsilon^4\big), \tag{25}$$

with phase velocity

$$c = c^{(0)} + \varepsilon^1 c^{(1)} + \varepsilon^2 c^{(2)} + \mathcal{O}\big(\varepsilon^3\big). \tag{26}$$

From our knowledge of the null space of $A(c^{(0)})$, keeping in mind the type of solution we seek, we set,

$$\begin{pmatrix} \eta^{(1)} \\ \xi^{(1)} \end{pmatrix} = a_1 \psi_1\big(c^{(0)}, k_1\big) + a_2 \psi_1\big(c^{(0)}, k_2\big), \tag{27}$$

where $(a_1, a_2) \in \mathbf{R}^2(a)$ are amplitude parameters and ψ_1 is given by (9). Using this Ansatz in the full traveling wave water wave problem (5) and equating terms at various powers of ε one can find relationships that describe the terms $c^{(j)}$. We begin with order one.

Proposition 4.2. *By equating the Taylor coefficients of $F(u, c) = 0$ at order ε^1 one arrives at the following equation for $(\eta^{(1)}, \xi^{(1)})^{\mathrm{T}}$,*

$$\begin{pmatrix} g & c^{(0)} \cdot \nabla_x \\ -c^{(0)} \cdot \nabla_x & G_0 \end{pmatrix} \begin{pmatrix} \eta^{(1)} \\ \xi^{(1)} \end{pmatrix} = \begin{pmatrix} 0 \\ 0 \end{pmatrix}. \tag{28}$$

Since $\psi_1(c^{(0)}, k_j) \in X_1$ this is consistent with the choice of $(\eta^{(1)}, \xi^{(1)})^{\mathrm{T}}$ of (27).

At second order we get the following system, which will imply that $c^{(1)} = 0$.

Proposition 4.3. *Equating terms in the expansion of $F(u, c) = 0$ at order ε^2 one arrives at the following system for $(\eta^{(2)}, \xi^{(2)})^{\mathrm{T}}$,*

$$\begin{pmatrix} g & c^{(0)} \cdot \nabla_x \\ -c^{(0)} \cdot \nabla_x & G_0 \end{pmatrix} \begin{pmatrix} \eta^{(2)} \\ \xi^{(2)} \end{pmatrix} = \begin{pmatrix} -c^{(1)} \cdot \nabla_x \xi^{(1)} - \frac{1}{2}\big(|\nabla_x \xi^{(1)}|^2 + (G_0 \xi^{(1)})^2\big) \\ c^{(1)} \cdot \nabla_x \eta^{(1)} - G_1(\eta^{(1)}) \xi^{(1)} \end{pmatrix}. \tag{29}$$

Enforcing the solvability condition we deduce that $c^{(1)} = 0$ and that,

$$\begin{aligned} \eta^{(2)} \;=\; & M(0) + M(2k_1)\cos(2k_1 \cdot x) + M(2k_2)\cos(2k_2 \cdot x) \\ & + M(k_1 + k_2)\cos\big((k_1 + k_2) \cdot x\big) + M(k_1 - k_2)\cos\big((k_1 - k_2) \cdot x\big) \end{aligned} \tag{30}$$

and

$$\begin{aligned} \xi^{(2)} \;=\; & N(2k_1)\sin(2k_1 \cdot x) + N(2k_2)\sin(2k_2 \cdot x) \\ & + N(k_1 + k_2)\sin\big((k_1 + k_2) \cdot x\big) + N(k_1 - k_2)\sin\big((k_1 - k_2) \cdot x\big). \end{aligned} \tag{31}$$

The coefficients $M(k)$, $N(k)$ $(k \neq k_1, k_2)$ are quadratic polynomial functions of the amplitudes $a(j)$, $j = 1, 2$, which are given in Appendix B.

The condition on $c^{(1)}$ comes from a Fredholm alternative. The inner product of the right-hand side with each of the null vectors shows that $c^{(1)} \cdot k_1 = 0$ and $c^{(1)} \cdot k_2 = 0$, implying $c^{(1)} = 0$ by the independence of k_1 and k_2.

The previous result is not surprising as bifurcation branches often intersect in such a tangential fashion. Meaningful higher order information comes from the third order analysis.

Proposition 4.4. *At order ε^3 one finds the system for $(\eta^{(3)}, \xi^{(3)})^{\mathrm{T}}$,*

$$\begin{pmatrix} g & c^{(0)} \cdot \nabla_x \\ -c^{(0)} \cdot \nabla_x & G_0 \end{pmatrix} \begin{pmatrix} \eta^{(3)} \\ \xi^{(3)} \end{pmatrix} = \begin{pmatrix} -c^{(2)} \cdot \nabla_x \xi^{(1)} - (\nabla_x \xi^{(1)}) \cdot (\nabla_x \xi^{(2)}) - (G_0 \xi^{(1)})(G_0 \xi^{(2)} + G_1(\eta^{(1)}) \xi^{(1)}) \\ c^{(2)} \cdot \nabla_x \eta^{(1)} - G_1(\eta^{(2)}) \xi^{(1)} - G_1(\eta^{(1)}) \xi^{(2)} - G_2(\eta^{(1)}) \xi^{(1)} \end{pmatrix}. \tag{32}$$

Enforcing the solvability condition we deduce that $c^{(2)}$ satisfies the following pair of linear equations,

$$k_1 \cdot c^{(2)} = \frac{-(c^{(0)} \cdot k_1) v_1 + g w_1}{2 a_1 g (c^{(0)} \cdot k_1)}, \tag{33a}$$

$$k_2 \cdot c^{(2)} = \frac{-(c^{(0)} \cdot k_2) v_2 + g w_2}{2 a_2 g (c^{(0)} \cdot k_2)}. \tag{33b}$$

The coefficients v_1, v_2, w_1, and w_2 are cubic polynomials in $a(j)$, $j = 1, 2$, which are given in Appendix B.

In principle the expressions for the coefficients $(\eta^{(3)}, \xi^{(3)})$ can be derived from Proposition 4.4. The apparent singularity in (33a) (respectively (33b)) as a_1 tends to zero (respectively a_2) has to do with the intersection of the bifurcation surfaces S_1 and S_3 (respectively S_2 and S_3), which is in fact regular. Inspection of the formulae shows that the expressions for $c^{(2)} \cdot k_1$ are well defined for $a_2 = 0$, which describes the surface S_2, and furthermore the limits $c^{(2)} \cdot k_1$, $c^{(2)} \cdot k_2$ exist as a_2 tends to zero, for fixed $a_1 \neq 0$. The analog statement holds for the intersection of S_2 and S_3.

4.3. Numerical calculations of short-crested wave bifurcation surfaces

The continuation method for numerical bifurcation theory is not naturally designed to construct bifurcation surfaces, and it has to be modified for the task. In particular at a bifurcation point $(0, c^{(0)})$ there is a full tangent plane $T(S_3)$ of possible initial vectors (a_1, a_2) from which to generate a parameter family of solutions. Furthermore one needs to know the behavior of the phase velocity $c = c(a)$, at least to lowest order. Our method of calculation is to set an initial tangent direction $V \in \mathbf{R}^2(a)$, and use a one-dimensional continuation method to construct a curve in the bifurcation surface S_3 parametrized by (pseudo-)arclength, for which the amplitude parameters satisfy $(a_1, a_2) = \sigma V$. Varying V through the unit circle in the tangent space $T(S_3)$ will in principle describe the bifurcation surface in (pseudo) geodesic polar coordinates about the bifurcation point $(0, c^{(0)})$. In order to determine the initial phase velocity $c \sim c^{(0)} + \sigma^2 c^{(2)}$ we use the formulae (33a) and (33b).

In practice this means that we start the continuation method at the bifurcation point $(0, c^{(0)})$ stemming from the fundamental domain T with the desired wave numbers $k_\ell \in \Gamma'$, and then follow a path $(a_1(\sigma), a_2(\sigma), c_1(\sigma), c_1(\sigma))$, where $(a_1(\sigma), a_2(\sigma)) = \sigma V$, and at the initial step

$$\begin{pmatrix} c_1(\sigma) \\ c_2(\sigma) \end{pmatrix} \sim \begin{pmatrix} c_1^{(0)} + c_1^{(2)} \sigma^2 \\ c_2^{(0)} + c_2^{(2)} \sigma^2 \end{pmatrix}. \tag{34}$$

We have performed an initial calculation to exhibit the capabilities of this method of tracing out the bifurcation surface. We chose a fundamental domain $\mathbf{T}$ to be the parallelogram with side lengths $R = 1$, with two of its interior angles $\Theta = \pi/3$, for which $c^{(0)} \sim (0.506457, 0.292403)^{\mathrm{T}}$. We took the initial amplitudes in the direction $V = (1, 2)^{\mathrm{T}}$, for which $\arctan(c_2^{(2)}/c_1^{(2)}) \sim 0.97024\pi$ gives the increment of phase velocity. This numerical calculation displays both the flexibility of the method toward computations on fundamental domains which are not rectangular, and to pick the initial nonlinear corrections to the phase velocity. A contour plot of a solution of reasonable amplitude and steepness that results from these runs is given in Fig. 8, for which we set $N_1 = N_2 = 24$, $m = 4$, $g = 1$, and $h = 0.1$.

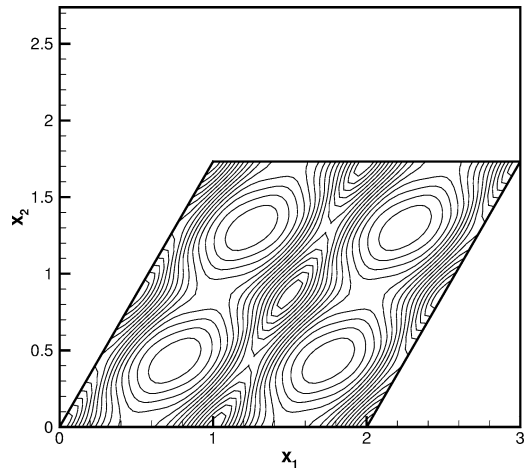

Fig. 8. Contour plot of $\eta(x_1, x_2)$ versus x_1 and x_2 on a skew fundamental domain ($\Theta = \pi/3$, $R = 1, a_1 = 1, a_2 = 2$).

4.4. Small divisor problem

There are many rigorous existence proofs for traveling water waves in the two-dimensional case, with or without surface tension, dating from the work of Levi-Civita [27] and Nekrasov [31]. In contrast to this, the three-dimensonal problem without surface tension exhibits the phenomenon of small divisors, and this has implications for any theoretical results on the problem. Indeed to date, the rigorous existence theory for three-dimensional multiply periodic traveling water waves is open.

In the problem of traveling water waves on $\mathbf{T} = \mathbf{R}^{n-1}/\Gamma$, for $n \geqslant 3$, analytic difficulties associated with solving (19) can occur in two places. One is that there may be infinitely many solutions $k \in \Gamma'$ to the dispersion relation (20), resulting in a Lyapunov–Schmidt decomposition with null space X_1 which is infinite dimensional. This corresponds to the problem of having to satisfy infinitely many simultaneous compatibility conditions. More seriously however is the second problem, associated with inverting the nonlinear equation (22) on the complement $X_1^{\perp}$ of the null space. The linearized operator around the trivial solution, in a basis of Fourier modes on $L^2(\mathbf{T})$, is expressed as

$$\partial_u F(0, 0; c) = \operatorname{diag}_{2\times 2} \hat{A}_k(c), \tag{35}$$

where $\hat{A}_k(c)$ is given in (7). Thus the spectrum of the linear problem is the closure of the set $\Sigma(c) = \bigcup_{k\in\Gamma'}\{\mu_+(k), \mu_-(k)\}$, with

$$\mu_{\pm}(k) = \frac{g + G_0(k)}{2}\left(1 \pm \sqrt{1 - \frac{4\Delta(k, c)}{(g + G_0(k))^2}}\right), \tag{36}$$

where $G_0(k) = |k|\tanh(h|k|)$ and $\Delta(k, c) = gG_0(k) - (c \cdot k)^2$. In order to exhibit the small divisor problem in the present setting, we will show that the set $\Sigma(c)$ is dense on a ray on the real axis, which in particular includes the point $\mu = 0$. It follows that the linearized operator $\partial_u F$ is not boundedly invertible from $X_1^{\perp} \subseteq H^r(\mathbf{T})$ to $Y_1^{\perp} \subseteq H^s(\mathbf{T})$ for any choice of Sobolev spaces $H^r(\mathbf{T})$, $H^s(\mathbf{T})$. It follows that Eq. (22) cannot be solved directly by a standard implicit function theorem.

Proposition 4.5. *Let $n \geqslant 3$. For any lattice $\Gamma \subseteq \mathbf{R}^{n-1}$ and for any $c \in \mathbf{R}^{n-1}$, the set $\Sigma(c)$ is dense in the ray $(-\infty, g] \subseteq \mathbf{R}$. In particular the point $\mu = 0$ lies in the closure $\overline{\Sigma}(c)$.*

Proof. Consider the curves $\Gamma_A \subseteq \mathbf{R}^2(k)$ defined by

$$\Gamma_A = \big\{k\colon\ \Delta(k, c) = A\big(G_0(k) + g\big)\big\}.$$

Along Γ_A we have $(g - A)G_0(k) - gA = (c \cdot k)^2 \geqslant 0$, and thus Γ_A is unbounded as long as $-\infty < A < g$. We will show that for such A, in a R-tubular neighborhood of Γ_A the eigenvalues $\mu_-(k) \sim A$ as $|k| \to \infty$. When R is large enough so that the tubular neighborhood contains infinitely many lattice points of Γ', this implies that $A \in \overline{\Sigma}(c)$. In particular, it suffices to take $R > \operatorname{diam}(\mathbf{T}')$, where $\mathbf{T}'$ is any fundamental domain for the dual torus $\mathbf{R}^2(k)/\Gamma'$.

Along an unbounded component of the curve Γ_A itself, we have

$$\mu_-(k) = \frac{g+G_0(k)}{2}\left(1-\sqrt{1-\frac{4\Delta(k,c)}{(g+G_0(k))^2}}\right) = \frac{g+G_0(k)}{2}\left(1-\sqrt{1-\frac{4A(G_0(k)+g)}{(g+G_0(k))^2}}\right)$$
$$\sim \frac{G_0(k)+g)}{2}\left(\frac{2A}{G_0(k)+g}\right) = A.$$

Furthermore, the unbounded components of the curves Γ_A are asymptotic to the parabolas

$$(c\cdot k)^2 = (g-A)|k|$$

whose semiminor axes are aligned with c. Given any two other constants $A_1 < A < A_2 < g$, the distance between their repective curves Γ_{A_1} and Γ_{A_2} is increasing as $|k| \to \infty$. Therefore given any radius R and given $\kappa \in \Gamma_A$, the ball $B_R(\kappa)$ lies in between the curves Γ_{A_1} and Γ_{A_2} as long as $|\kappa|$ is taken sufficiently large. This concludes the proof. □

In principle, the presence of small divisors could make the behavior of our numerical scheme very difficult to control. However in practice, and for most of the relevant phase velocity vectors c, small divisors are relatively rare, despite the fact that they are dense according to Proposition 4.5. Over typical Fourier collocation discretizations of our spatial domain, which comprise up to 256×256 points in a region of $\Gamma' \subseteq \mathbf{R}^2(k)$, and with typical computations of the bifurcation point c_0, we have not encountered small eigenvalues under the tolerance of approximately 10^{-3}. The numerical scheme appears to converge for a good way along the bifurcation surfaces as long as N and m (the highest retained degree of Taylor polynomial in our approximation for $G(\eta)$) are fixed. Nonetheless, we do not expect an expression for the full perturbation series expansion of a solution surface to converge, or even to represent an asymptotic series, a similar phenomenon to that encountered in KAM theory, as well as in the theory of standing waves (see Concus [13]).

In the case of nonzero surface tension, the problem is more regular, there are no small divisors, and there are several rigorous results of existence [39,15,20]. In particular an analysis of three-dimensional traveling water waves with surface tension, including the case of resonance and multiple bifurcation branches, appears in the second of these references.

5. Hexagonal wave patterns

In this section we will focus on numerical calculations of three-dimensional short crested traveling wave patterns which are computed on large aspect ratio periodic fundamental domains. That is, the width of the fundamental domain $\mathbf{T}(\Gamma)$ in the direction of propagation c is small when compared to the length of the domain transverse to the direction of propagation. It is in this geometrical setting that Hammack et al. [21,22] observe hexagonal surface wave patterns in wave tank experiments in shallow water, which they show correspond very well to genus two solutions of the KP equation with appropriately chosen parameters.

Our first point in this section is to compute surface water waves for the full Euler equations in the shallow water regime. As per the bifurcation results of this paper, these solutions occur in bifurcation surfaces, and their principal components consist of two two-dimensional traveling wave fields intersecting at an oblique angle. The principal results are that our numerical simulations of the Euler equations with shallow depth $h = 0.01$ give wave patterns which are very similar to those observed by Hammack et al. These are of intermediate steepness, with flattened troughs and with prominant zig–zag ridges connecting an alternating field of principal crests, illustrated in Figs. 9 and 10. Additionally, our calculations are able to be continued to wave patterns of very large steepness, exhibiting large and very flat troughs and a very well defined pattern of alternating crests connected by ridges. A typical calculation on a fundamental domain with aspect ratio 1 : 11 is shown in Figs. 11 and 12 which is for depth $h = 0.01$. Similar computations have been given in Nicholls [34].

We also show that the bifurcation surface S_3 containing these solutions is in fact a connecting surface between two distinct families of two-dimensional Stokes wavetrains traveling at oblique angles to each other. Points on this bifurcation surface can be parametrized by the two amplitudes of the two principal Fourier modes contributing to solutions on this branch of solutions, which we are denoting a_1 and a_2. A curve on the bifurcation surface S_3 for which $a_1 = a_2$ gives rise to solutions whose phase velocity c and momentum (I_1, I_2) are parallel to the x_1-axis, which is the case in Figs. 9 and 11. With the same fundamental domain $\mathbf{T}(\Gamma)$ we have traced out a portion of the bifurcation surface S_3, letting the ratio of the two amplitudes $a_2/a_1 = \rho$ vary from one to zero. For $\rho = 0$ this results in the bifurcation curve of Stokes wavetrain solutions, progressing at an angle $\arctan(1/11)$ to the x_1-axis. The Fig. 13 plots a piece of the surface S_3, projected onto the three-dimensional parameter space $(c_1, c_2, \|u\|_2)$ (recall that S_3 naturally lies in the four-dimensional parameter space $X_1 \times \mathbf{R}^2_c$). Fig. 14 gives a succession of snapshots of solutions on this surface, at points for which ρ varies from one to zero, fixing the amplitude $|a|$. As is evident, the pattern moves from a case in which the contributions of the two wave trains are equal, through a set of solutions which are biased towards one of the two, to finally a two-dimensional Stokes periodic traveling wave. The momentum of the family of solutions moves continuously from being parallel to the x_1-axis to a limiting value normal to the crests of the Stokes waves.

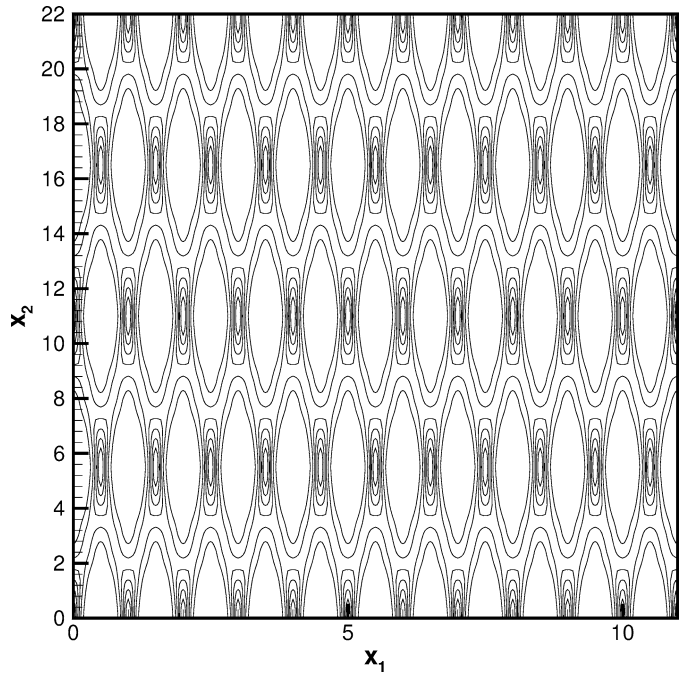

Fig. 9. Contour plot of a moderately steep hexagonal wave with $h = 0.01$.

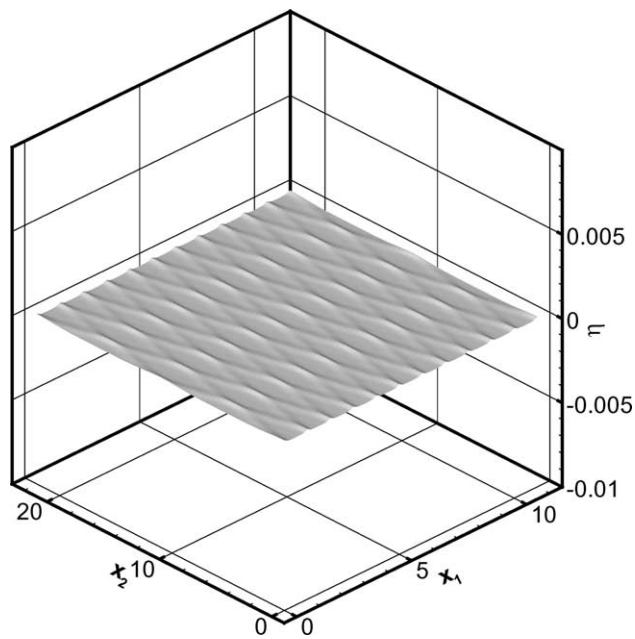

Fig. 10. Graph in perspective of a moderately steep hexagonal wave with $h = 0.01$. The vertical scaling is not exaggerated.

The second point exhibited by our numerical simulations of the full Euler equations is the fundamental dependence of the form of traveling wave solutions on the depth of the fluid domain. In the shallow water case $0 < h \ll 1$, the solutions are well modeled by the KP equation for moderate steepnesses, and have very definite hexagonal form. In contrast, for deep water the wave field is instead suited for a description by modulation theory and/or Zakharov's equations for an asymptotic description of nonlinear surface waves. Our numerical calculations show that there is a very strong tendency toward solutions in the form of families of long-crested rolls aligned in the direction of propagation, with both troughs and crests very elongated in the

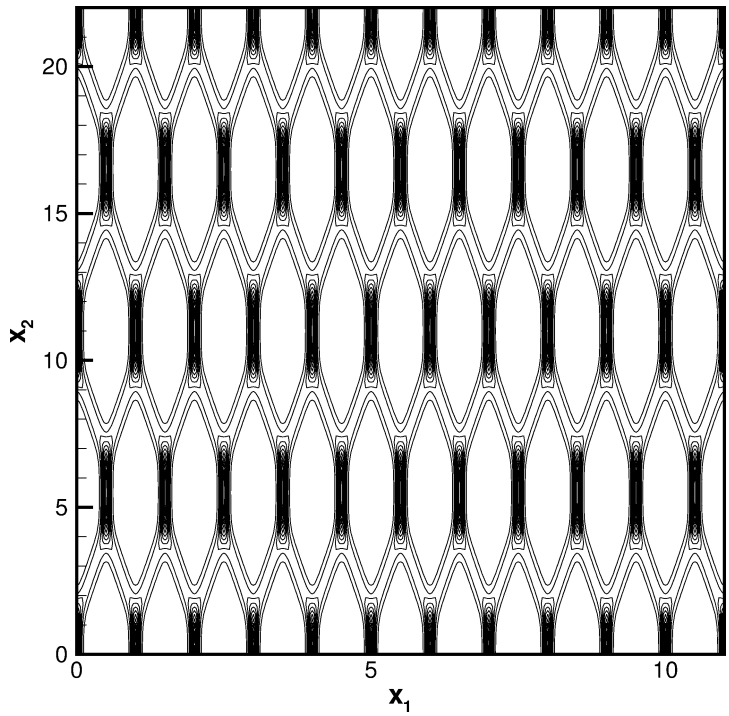

Fig. 11. Contour plot of a steep hexagonal wave with $h = 1/100$.

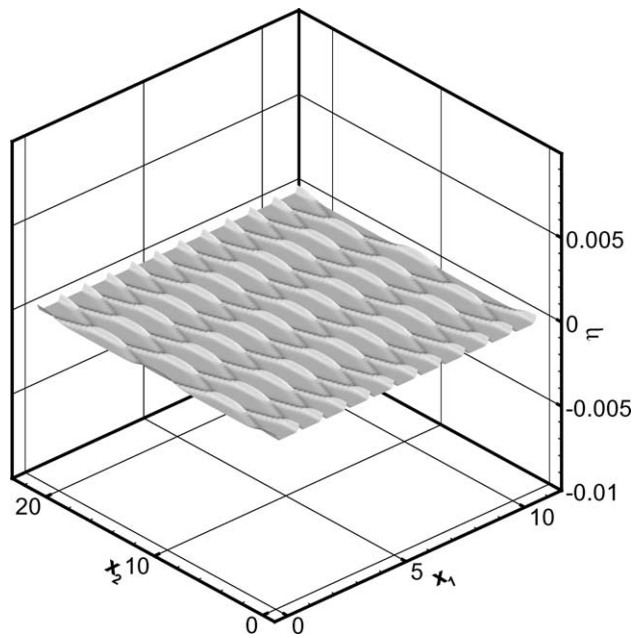

Fig. 12. Plot in perspective of a steep hexagonal wave with $h = 1/100$. The vertical scale is not exaggerated.

direction transverse to the phase velocity. In the direction of propagation however, these waves are only slightly deformed from a simple cosine profile, changing phase by π as one moves one's point of view along the x_2-axis through transition regions. There is only a slight tendency for sharpening of crests and broadening of troughs in these solutions. The degree of nonlinearity of these wave patterns is to be judged by the flatness of the troughs and crests in the transverse direction. We see this

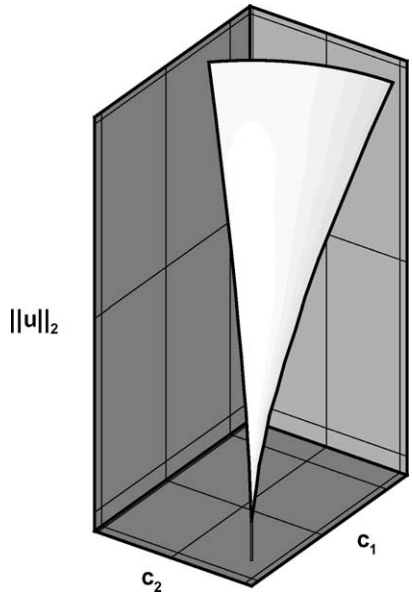

Fig. 13. Plot of a projection of the bifurcation surface, tangent to $T(S_3)$, with axes $\|u(x)\|_{L^2}$ vs. $c = (c_1, c_2)$ ($h = 1/100$).

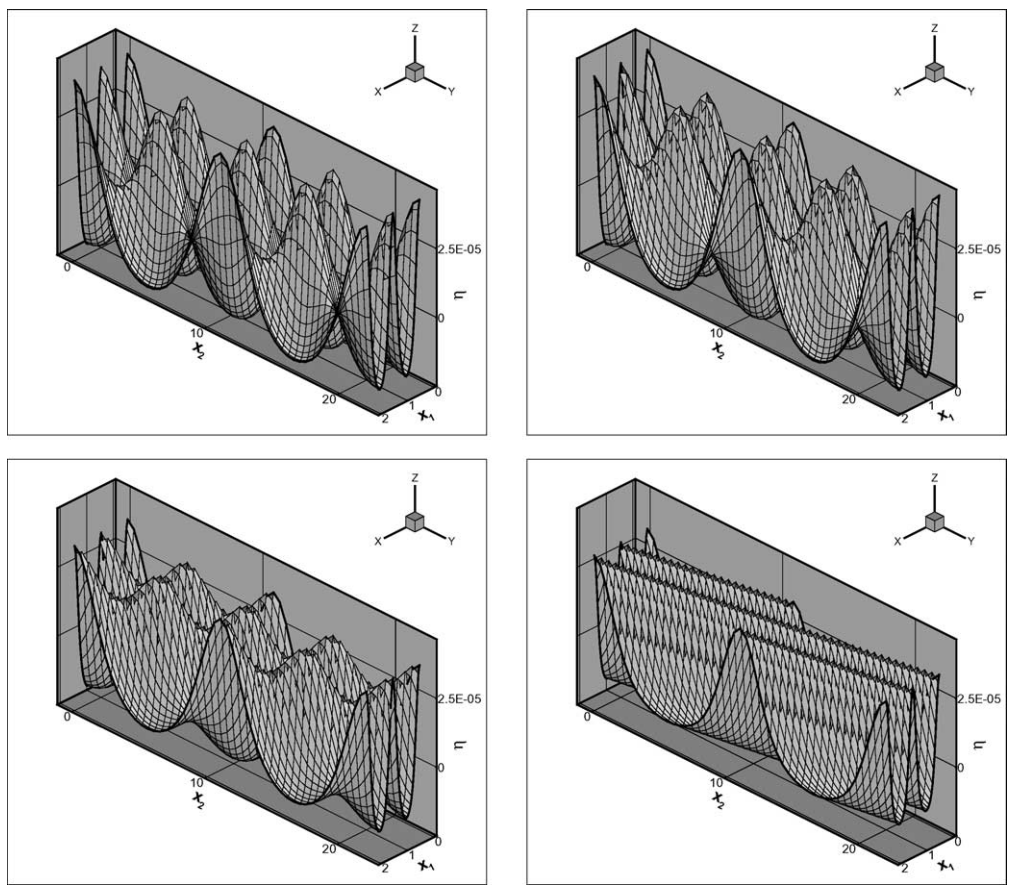

Fig. 14. Plots of $\eta(x)$ vs. x on the bifurcation surface S_3, varying $\vartheta = \arctan(a_2/a_1)$ from $\pi/4$ to 0, while fixing the amplitude $r = \sqrt{a_1^2 + a_2^2}$. The profile in the first figure is that of Fig. 9, with exagerated vertical scaling.

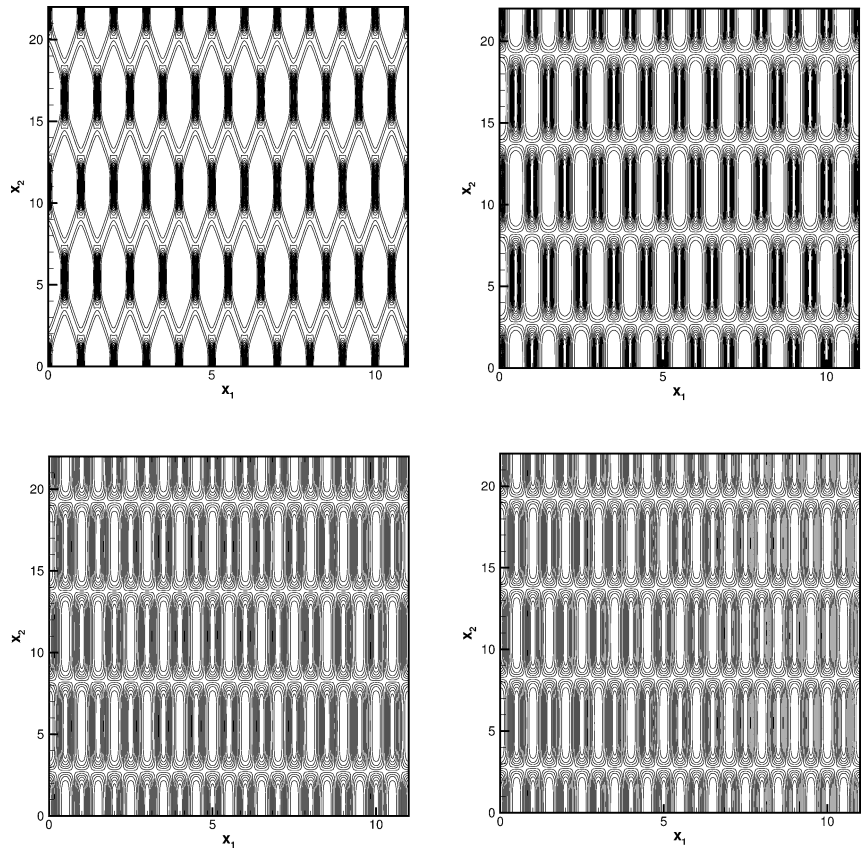

Fig. 15. Plots of traveling waves on an identical domain, as h is varied from 0.01 to $+\infty$ ($h = 0.01, 0.1, 1$ and $+\infty$). The first figure is that of Fig. 11.

shape dominating the characteristic form of traveling wave patterns (on the fundamental domain $\mathbf{T}(\Gamma)$ of aspect ration 1 : 11) already for depths $h = 0.1$, and their form changes only slightly as we increase h to infinity; this is illustrated in Fig. 15. This phenomenon is reported in the paper by Nicholls [34], and it is consistent with the wave tank experiments of J. Hammack and D. Henderson, and the observations of our focused research group [8] in work that is currently in progress. The transition region between hexagonal shapes, where $h \sim 0.01$ on our fundamental domain, and rolls, which are already dominant for $h = 0.1$, is an interesting area for investigation, and we feel that it merits further attention, through experimental as well as numerical work.

6. Conclusion

This paper develops a picture of the theory of two and three-dimensional periodic traveling water waves, from the viewpoint of perturbation analysis and numerical computations. In the two-dimensional case we recover the classical form of the Stokes traveling wavetrain, using the Hamiltonian formulation of the problem given in [18,54]. This includes bifurcation branches of solutions extending up to the Stokes solutions of extremal form, as well as secondary bifurcations. In three dimensions we develop an analogous theory of bifurcation of traveling waves from the constant state, arising from bifurcation points identified through solutions of the linearized equation. One of the main points that we make is that traveling wave solutions in three dimensions are expected to occur in general in two-dimensional bifurcation surfaces, arising from bifurcation points corresponding to two linear wavetrains with independent wavevectors. The structure of families of solutions near a simple bifurcation point is more complicated than for problems of simple bifurcation with one parameter, comprising a number of intersecting nontrivial solution surfaces as well as the surface describing the quiescent state. In cases of bifurcation points of higher multiplicity, solution families are expected to exist as given by the variational arguments of [15]. These are parametrized locally by the two components of the horizontal momentum, at least at nonsingular points of the bifurcation surface.

Our three-dimensional numerical computations have mostly focused on fundamental domains with relatively large aspect ratio. The resulting doubly periodic traveling wave solutions have different characteristics in the case of shallow water as compared with the deep water case. In shallow water, periodic traveling waves tend to form large flat troughs separated by steep and well localized ridges, giving rise to a pattern of hexagons in the free surface profile. This result is compatible with the experimental observations and KP modeling of [22,21]. In contrast, in deep water the periodic traveling waves tend to form long rolls aligned perpendicularly to the phase velocity. In the direction of motion, the variation in the height of the free surface is not far from sinusoidal, however in the direction orthogonal to this, the crests and troughs are significantly elongated. The transition regime in depth between these two cases is still under investigation.

A third traveling wave phenomenon of interest is the formation of crescent-shaped patterns in periodic wave fields in resonant situations in which there are more than two wave vectors k_j with the same linear phase velocity vector $c^{(0)}$. The resulting wave patterns are very beautiful, exhibiting alternating peaked crests and cols along a principal ridge, with crescent-shaped cirques trailing behind each crest. This phenomenon has been observed experimentally by Su et al. [47], Su [48] and Collard and Caulliez [12], and attempts to simulate this phenomenon numerically have appeared in Meiron et al. [30], Milewski and Keller [29], and more recently by Shrira, Badulin and Kharif [44] and Annakov and Shrira [3] (see the recent review article by Dias and Kharif [19]). The photographs in [47] and [48] showed at least two different cases of crescent-shaped waves, both of which possess crests in the solution which are not individually symmetric under reflection of the solution in a plane orthogonal to the phase velocity. In one case the solution had co-existing crescent-shaped features facing forwards with almost identical crescent-shaped features facing backwards. In the second and more highly nonlinear case, all of the crescent-shaped features are facing forwards. It is expected that these solutions are closely related to a five-wave resonance in the water wave Hamiltonian, as well as the instability of the Stokes wavetrain for large momenta [14]. The bifurcation problem for such crescent-shaped traveling waves is resonant, the null space of the linearized operator has higher than the minimum dimension, and there are extra parameters to determine in order to pick out the nonlinear solution branches which originate tangentially to this null space. Because of this, the numerical calculations of these solution branches are more difficult, and though it is an appealing problem, we have not yet been successful in applying our method to this case.

We note that the analytic component of the proof of existence of doubly periodic traveling water waves without surface tension is not complete, due to the presence of small divisors in the problem. A complete discussion of existence results for doubly periodic solutions in the case of nonzero surface tension, including an analysis of the case of linear resonance and resonant bifurcation, appears in [15].

Acknowledgements

W. Craig acknowledges research support from the Canada Research Chairs Program, the NSERC through grant number 238452-01 and the NSF through grant number DMS-0070218.

D.P. Nicholls acknowledges research support from the NSF through grant DMS-0196452.

Appendix A. The Dirichlet–Neumann operator

In two-dimensions it is known that the Dirichlet–Neumann operator is analytic as a function of η if the supremum norm and Lipschitz norm of η are bounded by a constant [11]. In general n dimensions the same conclusion is true if the supremum norm of the first derivatives of η is bounded by a constant [16,32,15]. As a consequence, for relatively small $|\eta|_{C^1}$ we can write $G(\eta)$ in terms of a convergent Taylor series expansion,

$$G(\eta) = \sum_{j=0}^{\infty} G_j(\eta), \tag{37}$$

where each term $G_j(\eta)$ of the Taylor series is homogeneous of degree j. The zeroth order term, corresponding to the case of a quiescent fluid $\eta = 0$, is

$$G_0\xi(x) = |D_x| \tanh\big(h|D_x|\big)\xi(x), \tag{38}$$

where $D_x = -\mathrm{i}\nabla_x$, [18]. A recursion formula for the jth term in this expansion is given in Craig and Sulem [18] in two-dimensions, and the straightforward generalization to three and n dimensions was derived by Schanz [43] and Nicholls [33], respectively. These formulae are useful from our perspective in their application to Fourier pseudospectral methods for numerical approaches to the water wave problem. With periodic boundary conditions and the explicit appearance of Fourier multiplier terms $D_x = -\mathrm{i}\partial_x$, $|D_x|$ and G_0 the method is not difficult to imagine, and the details are described in [18,33].

It turns out that the formulae adjoint to that of [18] is more effective in computations of the Dirichlet–Neumann operator. The point is that a recursive implementation of the calculation of the action of $G_j(\eta)\xi$ can be implemented in terms of concatenations of multiplication operations and Fourier multiplication operations on ξ and on $G_\ell(\eta)\xi$ for $\ell < j$, all of which are vector operations. Expressions for the matrix components of the operator $G(\eta)$ itself need not be computed and stored. A naïve count indicates that if the values of the vectors $G_\ell(\eta)\xi$ for $\ell < j$ are in storage, then the number of operations that are necessary to compute $G_j(\eta)\xi$ is $(j+1)\times 3N \times 2N\log(N)$, where N is the number of operations needed to perform a multiplication, and $N\log(N)$ is the number of operations to perform a fast Fourier transform. In the present work we take advantage of this fact in our numerical calculations. Using the adjoint formulae, the resulting recursion for the Dirichlet–Neumann operator is given as follows: for $j = 2r > 0$,

$$\begin{aligned} G_{2r}(\eta) \;=\; & \frac{1}{(2r)!}G_0\big(|D_x|^2\big)^{r-1}D_x\cdot\eta^{2r}D_x - \sum_{s=0}^{r-1}\frac{1}{(2(r-s))!}\big(|D_x|^2\big)^{r-s}\eta^{2(r-s)}G_{2s}(\eta) \\ & - \sum_{s=0}^{r-1}\frac{1}{(2(r-s)-1)!}G_0\big(|D_x|^2\big)^{r-s-1}\eta^{2(r-s)-1}G_{2s+1}(\eta), \end{aligned} \tag{39}$$

and, for $j = 2r-1 > 0$,

$$\begin{aligned} G_{2r-1}(\eta) \;=\; & \frac{1}{(2r-1)!}\big(|D_x|^2\big)^{r-1}D_x\cdot\eta^{2r-1}D_x - \sum_{s=0}^{r-1}\frac{1}{(2(r-s)-1)!}G_0\big(|D_x|^2\big)^{r-s-1}\eta^{2(r-s)-1}G_{2s}(\eta) \\ & - \sum_{s=0}^{r-2}\frac{1}{(2(r-s-1))!}\big(|D_x|^2\big)^{r-s-1}\eta^{2(r-s-1)}G_{2s+1}(\eta). \end{aligned} \tag{40}$$

Computations of the Dirichlet–Neumann operator via the adjoint formulae (39) and (40) are substantially faster and more memory conservative that those in the matrix form of the original formulae for $G_l(\eta)$ of [18].

Appendix B. Coefficients from calculation of Section 4.2

This section resolves the coefficients presented in Section 4.2 which were generated by a straightforward, if somewhat tedious, perturbation expansion to orders two and three respectively.

In regards to Proposition 4.3, the coefficients $M(k)$, $N(k)$ $(k \neq k_1, k_2)$ are determined by the linear systems,

$$\begin{pmatrix} g & (c^{(0)}\cdot k) \\ (c^{(0)}\cdot k) & |k|\tanh(h|k|) \end{pmatrix}\begin{pmatrix} M(k) \\ N(k) \end{pmatrix} = \begin{pmatrix} P(k) \\ Q(k) \end{pmatrix}, \tag{41}$$

where the only nonzero coefficients $P(k)$ and $Q(k)$ are

$$P(0) = -\frac{1}{4}g^2\big[a_1^2\big(|k_1|^2 + \widehat{G}_0(k_1)^2\big) + a_2^2\big(|k_2|^2 + \widehat{G}_0(k_2)^2\big)\big], \tag{42a}$$

$$P(2k_1) = -\frac{1}{4}g^2a_1^2\big[|k_1|^2 - \widehat{G}_0(k_1)^2\big], \tag{42b}$$

$$P(2k_2) = -\frac{1}{4}g^2a_2^2\big[|k_2|^2 - \widehat{G}_0(k_2)^2\big], \tag{42c}$$

$$P(k_1+k_2) = -\frac{1}{2}g^2a_1a_2\big[(k_1\cdot k_2) - \widehat{G}_0(k_1)\widehat{G}_0(k_2)\big], \tag{42d}$$

$$P(k_1-k_2) = -\frac{1}{2}g^2a_1a_2\big[(k_1\cdot k_2) + \widehat{G}_0(k_1)\widehat{G}_0(k_2)\big], \tag{42e}$$

and

$$Q(2k_1) = ga_1^2\big(c^{(0)}\cdot k_1\big)\left[|k_1|^2 - \frac{1}{2}\,\widehat{G}_0(k_1)\widehat{G}_0(2k_1)\right], \tag{43a}$$

$$Q(2k_2) = ga_2^2\big(c^{(0)}\cdot k_2\big)\left[|k_2|^2 - \frac{1}{2}\,\widehat{G}_0(k_2)\widehat{G}_0(2k_2)\right], \tag{43b}$$

$$Q(k_1+k_2) = \frac{1}{2}ga_1a_2\big\{\big(c^{(0)}\cdot k_1\big)\big[|k_2|^2 + (k_1\cdot k_2) - \widehat{G}_0(k_2)\widehat{G}_0(k_1+k_2)\big]$$

$$+\big(c^{(0)}\cdot k_2\big)\big[|k_1|^2+(k_1\cdot k_2)-\widehat{G}_0(k_1)\widehat{G}_0(k_1+k_2)\big]\big\}, \tag{43c}$$

$$Q(k_1-k_2)=\frac{1}{2}ga_1a_2\big\{\big(c^{(0)}\cdot k_1\big)\big[-|k_2|^2+(k_1\cdot k_2)+\widehat{G}_0(k_2)\widehat{G}_0(k_1-k_2)\big]$$
$$+\big(c^{(0)}\cdot k_2\big)\big[|k_1|^2-(k_1\cdot k_2)-\widehat{G}_0(k_1)\widehat{G}_0(k_1-k_2)\big]\big\}. \tag{43d}$$

The calculations for $P(k)$ and $Q(k)$ are a straightforward application of double and half angle formulae. The solution formula for $M(k)$ and $N(k)$ comes from solving the system $A(c^{(0)})(M,N)^{\mathrm{T}}=(P,Q)^{\mathrm{T}}$ at each of the wave numbers $k_1\pm k_2$, $2k_1$ and $2k_2$.

In regards to Proposition 4.4, the coefficients v_1, v_2, w_1, and w_2 are given by the following formulas.

$$v_1=\frac{1}{2}g\Big\{a_1\big[2|k_1|^2+\widehat{G}_0(k_1)\widehat{G}_0(2k_1)\big]N(2k_1)+a_2\big[|k_2|^2+(k_1\cdot k_2)+\widehat{G}_0(k_2)\widehat{G}_0(k_1+k_2)\big]N(k_1+k_2)$$
$$+a_2\big[-|k_2|^2+(k_1\cdot k_2)-\widehat{G}_0(k_2)\widehat{G}_0(k_1-k_2)\big]N(k_1-k_2)$$
$$-a_1\widehat{G}_0(k_1)Q(2k_1)-a_2\widehat{G}_0(k_2)\big[Q(k_1+k_2)+Q(k_1-k_2)\big]$$
$$-\frac{1}{2}g\big[a_1^3\big(c^{(0)}\cdot k_1\big)|k_1|^2\widehat{G}_0(k_1)+2a_1a_2^2\big(c^{(0)}\cdot k_2\big)(k_1\cdot k_2)\widehat{G}_0(k_2)\big]\Big\}, \tag{44a}$$

$$v_2=\frac{1}{2}g\Big\{a_2\big[2|k_2|^2+\widehat{G}_0(k_2)\widehat{G}_0(2k_2)\big]N(2k_2)+a_1\big[|k_1|^2+(k_1\cdot k_2)+\widehat{G}_0(k_1)\widehat{G}_0(k_1+k_2)\big]N(k_1+k_2)$$
$$+a_1\big[|k_1|^2-(k_1\cdot k_2)+\widehat{G}_0(k_1)\widehat{G}_0(k_1-k_2)\big]N(k_1-k_2)$$
$$-a_2\widehat{G}_0(k_2)Q(2k_2)-a_1\widehat{G}_0(k_1)\big[Q(k_1+k_2)+Q(k_1-k_2)\big]$$
$$-\frac{1}{2}g\big[a_2^3\big(c^{(0)}\cdot k_2\big)|k_2|^2\widehat{G}_0(k_2)+2a_1^2a_2\big(c^{(0)}\cdot k_1\big)(k_1\cdot k_2)\widehat{G}_0(k_1)\big]\Big\}, \tag{44b}$$

$$w_1=\frac{1}{2}\Big\{2a_1g\big[|k_1|^2-\widehat{G}_0(k_1)^2\big]M(0)+a_1g\big[|k_1|^2-\widehat{G}_0(k_1)^2\big]M(2k_1)$$
$$+a_2g\big[(k_1\cdot k_2)+\widehat{G}_0(k_1)\widehat{G}_0(k_2)\big]M(k_1+k_2)+a_2g\big[(k_1\cdot k_2)-\widehat{G}_0(k_1)\widehat{G}_0(k_2)\big]M(k_1-k_2)$$
$$+a_1\big(c^{(0)}\cdot k_1\big)\big[-2|k_1|^2+\widehat{G}_0(k_1)\widehat{G}_0(2k_1)\big]N(2k_1)$$
$$+a_2\big(c^{(0)}\cdot k_2\big)\big[-|k_1|^2-(k_1\cdot k_2)+\widehat{G}_0(k_1)\widehat{G}_0(k_1+k_2)\big]N(k_1+k_2)$$
$$+a_2\big(c^{(0)}\cdot k_2\big)\big[-|k_1|^2+(k_1\cdot k_2)+\widehat{G}_0(k_1)\widehat{G}_0(k_1-k_2)\big]N(k_1-k_2)+2a_1g|k_1|^2\widehat{G}_0(k_1)S(0)$$
$$+\frac{1}{2}a_2g\big[(k_1\cdot k_2)\widehat{G}_0(k_1)-|k_1|^2\widehat{G}_0(k_2)\big]S(k_1+k_2)+\frac{1}{2}a_2g\big[(k_1\cdot k_2)\widehat{G}_0(k_1)+|k_1|^2\widehat{G}_0(k_2)\big]S(k_1-k_2)$$
$$-\widehat{G}_0(k_1)\big[a_1\big(c^{(0)}\cdot k_1\big)Q(2k_1)+a_2\big(c^{(0)}\cdot k_2\big)\big(Q(k_1+k_2)+Q(k_1-k_2)\big)\big]\Big\}, \tag{44c}$$

and finally w_2 is given by,

$$w_2=\frac{1}{2}\Big\{2a_2g\big[|k_2|^2-\widehat{G}_0(k_2)^2\big]M(0)+a_2g\big[|k_2|^2+\widehat{G}_0(k_2)^2\big]M(2k_2)+a_1g\big[(k_1\cdot k_2)+\widehat{G}_0(k_1)\widehat{G}_0(k_2)\big]M(k_1+k_2)$$
$$+a_1g\big[(k_1\cdot k_2)-\widehat{G}_0(k_1)\widehat{G}_0(k_2)\big]M(k_1-k_2)+a_2\big(c^{(0)}\cdot k_2\big)\big[-2|k_2|^2+\widehat{G}_0(k_2)\widehat{G}_0(2k_2)\big]N(2k_2)$$
$$+a_1\big(c^{(0)}\cdot k_1\big)\big[-|k_2|^2-(k_1\cdot k_2)+\widehat{G}_0(k_2)\widehat{G}_0(k_1+k_2)\big]N(k_1+k_2)$$
$$+a_1\big(c^{(0)}\cdot k_1\big)\big[|k_2|^2-(k_1\cdot k_2)+\widehat{G}_0(k_2)\widehat{G}_0(k_1-k_2)\big]N(k_1-k_2)+2a_2g|k_2|^2\widehat{G}_0(k_2)S(0)$$
$$+\frac{1}{2}a_1g\big[(k_1\cdot k_2)\widehat{G}_0(k_2)-|k_2|^2\widehat{G}_0(k_1)\big]S(k_1+k_2)+\frac{1}{2}a_1g\big[(k_1\cdot k_2)\widehat{G}_0(k_2)+|k_2|^2\widehat{G}_0(k_1)\big]S(k_1-k_2)$$
$$-\widehat{G}_0(k_2)\big[a_2\big(c^{(0)}\cdot k_2\big)Q(2k_2)+a_1\big(c^{(0)}\cdot k_1\big)\big(Q(k_1+k_2)-Q(k_1-k_2)\big)\big]\Big\}. \tag{44d}$$

In these formulae we use the following abbreviations:

$$S(0)=\frac{1}{2}\big(a_1^2\big(c^{(0)}\cdot k_1\big)^2+a_2^2\big(c^{(0)}\cdot k_2\big)^2\big), \tag{45a}$$

$$S(2k_1)=\frac{1}{2}a_1^2\big(c^{(0)}\cdot k_1\big)^2, \tag{45b}$$

$$S(2k_2) = \frac{1}{2}a_2^2\big(c^{(0)} \cdot k_2\big)^2, \tag{45c}$$

$$S(k_1 + k_2) = a_1 a_2 \big(c^{(0)} \cdot k_1\big)\big(c^{(0)} \cdot k_2\big), \tag{45d}$$

$$S(k_1 - k_2) = a_1 a_2 \big(c^{(0)} \cdot k_1\big)\big(c^{(0)} \cdot k_2\big). \tag{45e}$$

References

[1] E. Allgower, K. Georg, Numerical Continuation Methods, Springer-Verlag, Berlin, 1990. An introduction.
[2] C. Amick, J. Toland, On solitary water-waves of finite amplitude, Arch. Rational Mech. Anal. 76 (1981) 9–95.
[3] S.Y. Annenkov, V.I. Shrira, On the predictability of evolution of surface gravity and gravity-capillary waves, Phys. D 152/153 (2001) 665–675.
[4] C. Baesens, R.S. MacKay, Uniformly travelling water waves from a dynamical systems viewpoint: some insight into bifurcation from Stokes' family, J. Fluid Mech. 241 (1992) 333–347.
[5] T.J. Bridges, F. Dias, D. Menasce, Steady three-dimensional water-wave patterns on a finite-depth fluid, J. Fluid Mech. 436 (2001) 145–175.
[6] B. Buffoni, E.N. Dancer, J.F. Toland, The sub-harmonic bifurcation of Stokes waves, Arch. Rational Mech. Anal. 152 (2000) 241–271.
[7] C. Canuto, M. Hussaini, A. Quarteroni, T. Zang, Spectral Methods in Fluid Dynamics, Springer-Verlag, New York, 1988.
[8] J. Carter, W. Craig, B. Deconinck, J. Hammack, D. Henderson, D. Nicholls, H. Segur, C. Sulem, Personal communication among the focused research group on surface water waves: http://www.math.colostate.edu/deconinc/frgsurfacewaves.html.
[9] B. Chen, P.G. Saffman, Steady gravity-capillary waves on deep water. II. Numerical results for finite amplitude, Stud. Appl. Math. 62 (1980) 95–111.
[10] B. Chen, P.G. Saffman, Numerical evidence for the existence of new types of gravity waves of permanent form on deep water, Stud. Appl. Math. 62 (1980) 1–21.
[11] R. Coifman, Y. Meyer, Nonlinear harmonic analysis and analytic dependence, in: Pseudodifferential Operators and Applications, Notre Dame, IN, 1984, American Mathematical Society, 1985, pp. 71–78.
[12] F. Collard, G. Caulliez, Oscillating crescent-shaped water wave patterns, Phys. Fluids 11 (1999) 3195–3197.
[13] P. Concus, Standing capillary-gravity waves of finite amplitude, J. Fluid Mech. 14 (1962) 568–576. Corrigendum: J. Fluid Mech. 19 (1964) 264–266.
[14] W. Craig, On the Badulin, Kharif and Shrira model of resonant water waves, Phy. D 152–153 (2001) 434–450.
[15] W. Craig, D. Nicholls, Traveling two and three-dimensional capillary gravity water waves, SIAM J. Math. Anal. 32 (2000) 323–359.
[16] W. Craig, U. Schanz, C. Sulem, The modulation regime of three-dimensional water waves and the Davey–Stewartson system, Ann. Inst. H. Poincaré 14 (1997) 615–667.
[17] W. Craig, P. Sternberg, Symmetry of solitary waves, Comm. Partial Differential Equations 13 (1988) 603–633.
[18] W. Craig, C. Sulem, Numerical simulation of gravity waves, J. Comput. Phys. 108 (1993) 73.
[19] F. Dias, Ch. Kharif, Nonlinear gravity and capillary-gravity waves, Ann. Rev. Fluid Mech. 31 (1999) 301–346.
[20] M. Groves, A. Mielke, A spatial dynamics approach to three-dimensional gravity-capillary steady water waves, Proc. Roy. Soc. Edinburgh Sect. A 131 (2001) 83–136.
[21] J. Hammack, D. McCallister, N. Scheffner, H. Segur, Two-dimensional periodic waves in shallow water. Part 2: asymmetric waves, J. Fluid Mech. 285 (1995) 95.
[22] J. Hammack, N. Scheffner, H. Segur, Two-dimensional periodic waves in shallow water, J. Fluid Mech. 209 (1989) 567.
[23] J.K. Hunter, J.-M. Vanden-Broeck, Solitary and periodic gravity-capillary waves of finite amplitude, J. Fluid Mech. 134 (1983) 205–219.
[24] H.B. Keller, Lectures on numerical methods in bifurcation problems, Published for the Tata Institute of Fundamental Research, Bombay, 1987. With notes by A.K. Nandakumaran and Mythily Ramaswamy.
[25] O. Kimmoun, H. Branger, Ch. Kharif, On short-crested waves: experimental and analytical investigations, Eur. J. Mech. B Fluids 18 (1999) 889–930.
[26] C.W. Lenau, The solitary wave of maximum amplitude, J. Fluid Mech. 26 (1966) 309.
[27] T. Levi-Civita, Détermination rigoreuse des ondes permanentes d'ampleure finie, Math. Ann. 93 (1925) 264–314.
[28] M. Longuet-Higgins, M. Tanaka, On the crest instabilities of steep surface waves, J. Fluid Mech. 336 (1997) 51–68.
[29] P. Milewski, J.B. Keller, Three-dimensional water waves, Stud. Appl. Math. 97 (2) (1996) 149–166.
[30] D. Meiron, P. Saffman, H. Yuen, Calculation of steady three-dimensional deep-water waves, J. Fluid Mech. 124 (1982) 109.
[31] A.I. Nekrasov, The exact theory of steady state waves on the surface of a heavy fluid, Mathematics Research Center Report 813, University of Wisconsin, MA, 1967.
[32] D. Nicholls, Traveling gravity water waves in two and three dimensions, Ph.D. thesis, Brown University, 1998.
[33] D. Nicholls, Traveling water waves: Spectral continuation methods with parallel implementation, J. Comp. Phys. 142 (1) (1998) 224–240.
[34] D. Nicholls, On hexagonal gravity water waves, Math. Comput. Simulation 55 (2001) 567–575.
[35] D. Nicholls, F. Reitich, A new approach to analyticity of Dirichlet–Newmann operators, Proc. Roy. Soc. Edinburgh Sect. A 131 (2001) 1411–1433.

[36] D. Nicholls, F. Reitich, Stability of high-order perturbative methods for the computation of Dirichlet–Neumann Operators, J. Comput. Phys. 170 (2001) 276–298.
[37] D. Nicholls, F. Reitich, Analytic continuation of Dirichlet–Neumann operators, Numer. Math., to appear.
[38] P. Plotnikov, Nonuniqueness of solutions of the problem of solitary waves and bifurcation of critical points of smooth functionals, Math. USSR-Izv. 38 (1992) 333–357.
[39] J. Reeder, M. Shinbrot, Three-dimensional nonlinear wave interaction in water of constant depth, Nonlinear Anal. 5 (1981) 303–323.
[40] A.J. Roberts, Highly nonlinear short-crested water waves, J. Fluid Mech. 135 (1983) 310–321.
[41] A.J. Roberts, H. Peregrine, Notes on long-crested water waves, J. Fluid Mech. 135 (1983) 323–335.
[42] P. Saffman, H.C. Yuen, Three-dimensional waves on deep water, Adv. in Nonlinear Waves 11 (1985) 1–30.
[43] U. Schanz, On the evolution of gravity-capillary waves in three dimensions, Ph.D. thesis, University of Toronto, 1997.
[44] V.I. Shrira, S.I. Badulin, Ch. Karif, A model of water wave horse-shoe patterns, J. Fluid Mech. 318 (1996) 375–404.
[45] G.G. Stokes, On the theory of oscillatory waves, Cambridge Philos. Soc. Trans. 8 (1847) 441–455.
[46] D. Struik, Détermination rigoreuse des ondes irrotationelles périodiques dans un canal à profondeur finie, Math. Ann. 95 (1926) 595–634.
[47] M.-Y. Su, M. Bergin, P. Marler, R. Myrick, Experiments on nonlinear instabilities and evolution of steep gravity-wave trains, J. Fluid Mech. 124 (1982) 45.
[48] M.-Y. Su, Three-dimensional deep-water waves. Part I. Experimental measurement of skew and symmetric wave patterns, J. Fluid Mech. 124 (1982) 73.
[49] M. Tanaka, The stability of steep gravity waves, J. Phys. Soc. Japan 52 (1983) 3047–3055.
[50] J.M. Williams, Limiting gravity waves in water of finite depth, Philos. Trans. Roy. Soc. London Ser. A 302 (1466) (1981) 139–188.
[51] J.M. Witting, On the highest and other solitary waves, SIAM J. Appl. Math. 28 (1975) 700.
[52] H. Yamada, On the highest solitary wave, Rep. Res. Inst. Appl. Mech. 5 (1957) 53–67.
[53] Z.-H. Yang, H.B. Keller, A direct method for computing higher order folds, SIAM J. Sci. Statist. Comput. 7 (2) (1986) 351–361.
[54] V.E. Zakharov, Stability of periodic waves of finite amplitude on the surface of a deep fluid, J. App. Mech. Techn. Phys. 9 (1968) 190.
[55] J. Zufiria, Weakly nonlinear nonsymmetric gravity waves on water of finite depth, J. Fluid Mech. 180 (1987) 371–385.
[56] J. Zufiria, Nonsymmetric gravity waves on water of infinite depth, J. Fluid Mech. 181 (1987) 17–39.